The Astrophysical Journal, 626:680–697, 2005 June 20

PASSIVELY EVOLVING EARLY-TYPE GALAXIES AT $1.4 \lesssim z \lesssim 2.5$ IN THE HUBBLE ULTRA DEEP FIELD[1]

E. Daddi,[2,3] A. Renzini,[3] N. Pirzkal,[4] A. Cimatti,[5] S. Malhotra,[4] M. Stiavelli,[4] C. Xu,[4] A. Pasquali,[6] J. E. Rhoads,[4] M. Brusa,[7] S. di Serego Alighieri,[5] H. C. Ferguson,[4] A. M. Koekemoer,[4] L. A. Moustakas,[4] N. Panagia,[4] and R. A. Windhorst[8]

Received 2004 November 26; accepted 2005 March 3

ABSTRACT

We report on a complete sample of seven luminous early-type galaxies in the Hubble Ultra Deep Field (UDF) with spectroscopic redshifts between 1.39 and 2.47, and to $K_{AB} < 23$. Using the *BzK* selection criterion, we have preselected a set of objects over the UDF, which fulfill the photometric conditions for being passively evolving galaxies at $z > 1.4$. Low-resolution spectra of these objects have been extracted from the *Hubble Space Telescope* (*HST*) ACS grism data taken over the UDF by the Grism ACS Program for Extragalactic Science (GRAPES) project. Redshifts for the seven galaxies have been identified based on the UV feature at rest frame $2640 < \lambda < 2850$ Å. This feature is mainly due to a combination of Fe II, Mg I, and Mg II absorptions, which are characteristic of stellar populations dominated by stars older than ~0.5 Gyr. The redshift identification and the passively evolving nature of these galaxies is further supported by the photometric redshifts and by the overall spectral energy distribution (SED), with the ultradeep *HST* ACS NICMOS imaging revealing compact morphologies typical of elliptical/early-type galaxies. From the SED we derive stellar masses of $\gtrsim 10^{11} M_{\odot}$ and ages of ~1 Gyr. Their space density at $\langle z \rangle = 1.7$ appears to be roughly a factor of 2–3 smaller than that of their local counterparts, further supporting the notion that such massive and old galaxies are already ubiquitous at early cosmic times. Much smaller effective radii are derived for some of the objects, compared to local massive ellipticals, which may be due to morphological *K*-corrections, evolution, or the presence of a central pointlike source. Nuclear activity is indeed present in a subset of the galaxies, as revealed by the fact that they are hard X-ray sources, which suggests that active galactic nucleus (AGN) activity may have played a role in discontinuing star formation.

Subject headings: cosmology: observations — galaxies: evolution — galaxies: formation — galaxies: high-redshift

Online material: color figures

1. INTRODUCTION

In the local universe, as accurately measured by the Sloan Digital Sky Survey (SDSS; see, e.g., Baldry et al. 2004), passive early-type galaxies with stellar masses larger than $10^{11} M_{\odot}$ dominate the counts of most massive galaxies, being a factor of 3 more numerous than late-type galaxies above this mass threshold. About one-third of all the stars in galaxies in the local universe are hosted by such objects (Baldry et al. 2004). The process by which these galaxies formed is still unclear. At least some of them may have formed at relatively high redshifts in a process that, for its rapidity, is reminiscent of the monolithic collapse scenario (Eggen et al. 1962). On the other hand, others may have been assembled at relatively recent epochs, through merging of smaller subunits (Toomre 1977). The formation of massive spheroids is a central problem of current theories of galaxy formation (see, e.g., Loeb & Peebles 2003; Gao et al. 2004).

It is now well established that up to $z \sim 1$ a significant population of red passively evolving early-type galaxies can be found in the field among extremely red objects (EROs; Cimatti et al. 2002a; Yan et al. 2004b; see McCarthy 2004 for a review) together with dust-reddened systems. The EROs are highly clustered (Daddi et al. 2000a; McCarthy et al. 2001; Roche et al. 2002; Miyazaki et al. 2003; Brown et al. 2005; Georgakakis et al. 2005), as expected for the progenitors of local massive ellipticals (Daddi et al. 2001; Moustakas & Somerville 2002). The space density of $z \sim 1$ early-type galaxies is at least within a factor of 2 of the local value (Daddi et al. 2000b; Pozzetti et al. 2003; Bell et al. 2004; Caputi et al. 2004), implying a modest evolution from $z = 1$, especially for the most massive ones. Their stars appear fairly old ($\gtrsim$3 Gyr), suggesting even higher-formation redshifts, $z \gtrsim 2$ (Cimatti et al. 2002a; Treu et al. 2005).

On the other hand, physically motivated galaxy formation models based on hierarchical clustering within the ΛCDM framework (Cole et al. 2001; Kauffmann et al. 1999; Somerville et al. 2001) have so far been unable to account for the large space density of $z > 1$ red galaxies (Daddi et al. 2000b; Smith et al. 2001; Firth et al. 2002; Somerville et al. 2004; Glazebrook et al. 2004). These models result in widespread merging and associated star formation activity of massive galaxies at relatively low redshifts, and it is currently not fully clear what physical mechanism needs to be involved in order to terminate star formation

[1] Based on observations with the NASA/ESA *Hubble Space Telescope*, obtained at the Space Telescope Science Institute, which is operated by AURA, Inc, under NASA contract NAS 5-26555; also based on data collected at the European Southern Observatory, Chile.

[2] Spitzer Fellow, National Optical Astronomy Observatory, P.O. Box 26732, Tucson, AZ 85726; edaddi@noao.edu.

[3] European Southern Observatory, Karl-Schwarzschild-Strasse 2, D-85748 Garching, Germany.

[4] Space Telescope Science Institute, 3700 San Martin Drive, Baltimore, MD 21218.

[5] INAF—Osservatorio Astrofisico di Arcetri, Largo E. Fermi 5, Firenze, Italy.

[6] Institute of Astronomy, ETH Hönggerberg, CH-8093 Zurich, Switzerland.

[7] Max-Planck-Institut für Extraterrestrische Physik, D-85478 Garching, Germany.

[8] Department of Physics and Astronomy, Arizona State University, P.O. Box 871504, Tempe, AZ 85287-1504.

and produce the red colors of passive galaxies. Feedback processes, e.g., from the onset of active galactic nucleus (AGN) activity, seem to be a promising tool to achieve that (Granato et al. 2001, 2004; Springel et al. 2005). This strengthens the necessity to simultaneously trace the formation of galaxies and AGN activity in order to understand the link between assembly of stellar mass in galaxies and the growth of supermassive black holes (Magorrian et al. 1998; Ferrarese & Merritt 2000).

As little evolution in massive ($>10^{11}\ M_\odot$) field early-type galaxies is detected up to $z = 1$, it is necessary to push the investigation to the highest possible redshifts in order to further constrain the formation of early-type galaxies. Crucial questions to ask are (1) up to which redshift do passively evolving early-type galaxies exist, (2) what is their space density as a function of z, (3) what is their clustering, and (4) what is the environment in which they live (i.e., cluster vs. field)? Studying the highest redshift massive and passive objects, i.e., those presumably closest to the formation or assembly epoch, could in principle also reveal useful information for understanding the physical processes by which these galaxies were formed.

For almost a decade the unique example of a spectroscopically confirmed high-z passive galaxy beyond $z \sim 1.5$ has been 53W 091 at $z = 1.55$ (Dunlop et al. 1996; Spinrad et al. 1997). This object was preselected for being a radio galaxy; hence, it was virtually selected over the whole sky. Its very red colors suggested fairly old stellar populations, although with some controversies about detailed age (see, e.g., Nolan et al. 2001 and references therein). The North and South Hubble Deep Fields, with their extremely deep imaging data, prompted searches for $z > 1.5$ passive galaxy candidates (Treu et al. 1999; Stiavelli et al. 1999; Broadhurst & Bouwens 2000; Benítez et al. 1999); however, no such objects were eventually spectroscopically confirmed because of the faintness of the candidates in the optical domains and because optical spectroscopy from the ground is hampered by the presence of strong OH sky emission lines at the wavelengths where the main spectral features are redshifted. Now, over fields of a few ten to a few hundred arcmin^2, three groups have recently presented the discovery of several high-z passive galaxies. Cimatti et al. (2004) report four passive galaxies spectroscopically confirmed at $1.6 < z < 1.9$ in the K20 survey, from a region within the GOODS-South field. The ACS imaging revealed their compact early-type-galaxy–like morphologies. McCarthy et al. (2004) have redshifts for 20 passive objects in $1.3 < z < 2.15$ (eight of which are at $z > 1.5$) from the Gemini Deep Deep Survey. Saracco et al. 2005 confirm seven very massive old galaxies at $1.3 < z < 1.7$ from low-resolution near-IR spectroscopy. The latter two studies both lack *HST* morphology information.

While it is now established that a significant population of passive galaxies exist up to $z \sim 2$ at least, the availability of the Hubble Ultra Deep Field (UDF) data set, with ultimately deep and high spatial-resolution optical and near-IR imaging, offers a unique possibility for studying these high-z passive galaxies in some detail. As a part of our Grism ACS Program for Extragalactic Science (GRAPES), we have collected about 50 *HST* orbits of ACS G800L grism spectroscopy on the UDF (Pirzkal et al. 2004, hereafter P04). As discussed in more detail later in the paper, the *HST* ACS spectroscopy allows us to obtain much higher S/N ratios on the continuum than those reachable from the ground. In this paper, we have taken advantage of the GRAPES spectra to present spectroscopic confirmation for a sample of seven early-type galaxies at $1.4 < z < 2.5$ in the UDF and use the available multiwavelength data sets to study their properties.

The paper is organized as follows. In § 2 we comment on the usefulness of low-resolution spectra of passive galaxies, and a new spectral index is defined for their characterization. Section 3 discusses the color selection of $z > 1.4$ passive galaxy candidates. In § 4 redshift identifications are presented and discussed in detail. Morphological parameters of the seven objects are derived in § 5. Stellar population properties, including stellar masses and ages, are estimated in § 6. The issue of space-density evolution of passive early-type galaxies to $z = 2.5$ is discussed in § 7, while in § 8 the evolution of morphology is discussed. Section 9 presents the X-ray detection of two of the galaxies in our sample. Summary and conclusions are given in § 10.

We assume a Salpeter initial mass function (IMF) from 0.1 and 100 $M_\odot$, and a *Wilkinson Microwave Anisotropy Probe* (*WMAP*) flat cosmology with $\Omega_\Lambda,\ \Omega_M = 0.73,\ 0.27$ and $h = H_0(\mathrm{km\ s^{-1}\ Mpc^{-1}})/100 = 0.71$ (Spergel et al. 2003).

2. UV SPECTRA OF PASSIVE GALAXIES: THE Mg_{UV} FEATURE

The low resolution of the *HST* grism spectra does not allow us to detect individual absorption or emission lines (if not for large equivalent widths; Xu et al. 2005) whose identification generally yields redshift measurements in higher resolution spectroscopy. Nevertheless the GRAPES spectra are well suited for the identification of broad, low-resolution spectral features such as the strong breaks that are commonly found among old stellar populations. Figure 1 shows rest-frame UV spectra (the region generally accessible to GRAPES *HST* ACS for $1.4 < z < 2.5$ objects) from Bruzual & Charlot (2003) spectral synthesis models and from Kurucz models of stars (Kurucz 1979), smoothed to the typical resolution of our data. While the 4000 Å break and the 3600 Å Balmer break rapidly disappear beyond 1 μm for $z \gtrsim 1.4$, there are other strong age-dependent features in the UV that are detectable in relatively low resolution spectra. The most prominent one is a bump in the region 2640–2850 Å that is due to the combination of several strong absorption lines, including Mg II λ2800, which is the strongest one. The typical shape of this region was first used by Spinrad et al. (1997) to measure the redshift of the $z = 1.55$ passive galaxy and also more recently by Cimatti et al. (2004) and McCarthy et al. (2004). We have dubbed this feature the Mg_{UV} feature, and defined the Mg_{UV} index as

$$\mathrm{Mg_{UV}} = \frac{2\int_{2625}^{2725} f_\lambda\, d\lambda}{\int_{2525}^{2625} f_\lambda\, d\lambda + \int_{2725}^{2825} f_\lambda\, d\lambda}, \qquad (1)$$

where the integration ranges (see Fig. 1) are defined in Å. The Mg_{UV} feature is found to be almost independent of the spectral resolution for $R \gtrsim 50$, the typical rest-frame resolution of the spectra discussed in this paper, and on dust extinction. Figure 2 shows the age dependence of the Mg_{UV} feature for passive as well as active star-forming galaxies. The Mg_{UV} feature is a key fingerprint of the presence of passively evolving stellar populations because it is not present in young dust-reddened star-forming galaxies (Figs. 1 and 2), which can still produce similarly red overall colors for high dust extinction. Its secure detection therefore allows one to establish the nature of the sources by breaking the age/dusty degeneracy among red sources, as well as the measurement of the galaxy redshift.

3. PASSIVE $z > 1.4$ GALAXIES: SAMPLE SELECTION

In order to search for high-redshift, passively evolving galaxies among the $\gtrsim$10,000 galaxies detected in the UDF, we

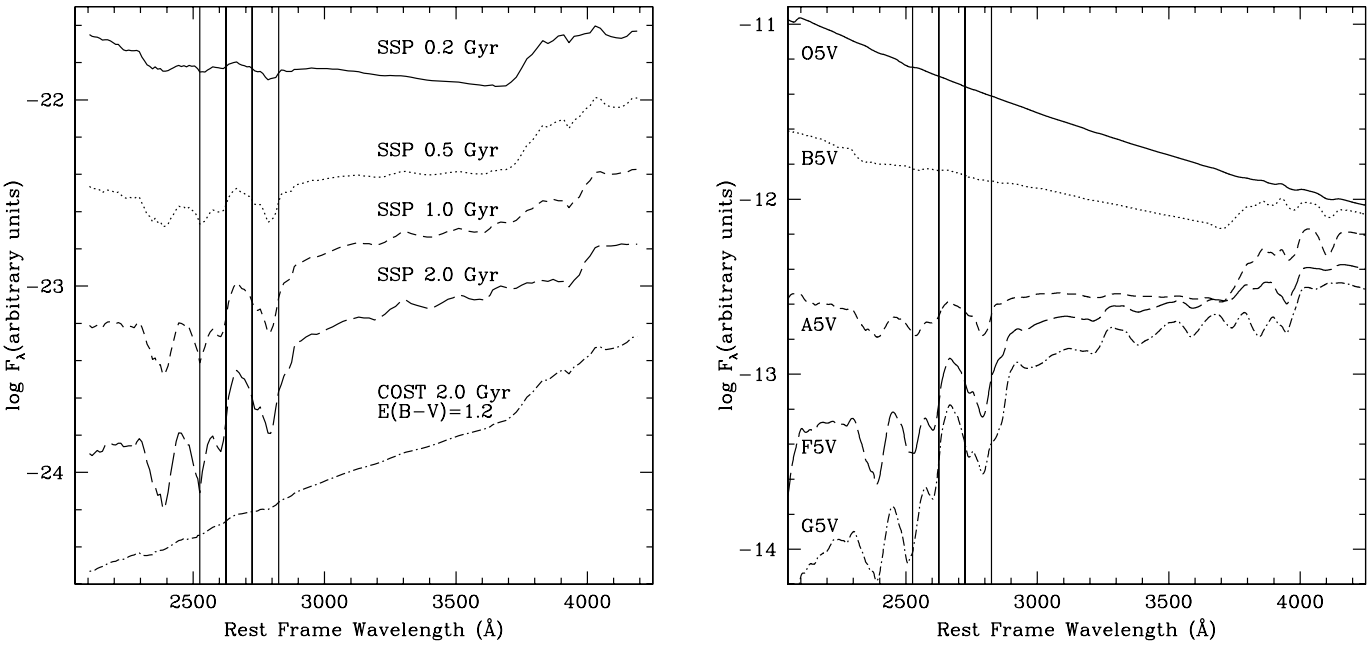

FIG. 1.—Mid-UV spectral energy distribution of galaxies from the Bruzual & Charlot (2003) library (*left*) and of stars from the Kurucz database (*right*), smoothed to ~50 Å rest-frame resolution, similar to the *HST* spectra of the objects analyzed in this paper. Old SSP galaxies or low-mass stars have very red spectra and a characteristic signature with a peak and a dip in the region 2640–2850 Å, mainly due to a combination of Fe II, Mg I, and Mg II absorption lines. This Mg_{UV} feature appears after a few hundred Myr of passive evolution (visible in A-type stars or later) and gets stronger as age increases (notice the 2 order of magnitude UV continuum dimming for SSP galaxies from 0.2 to 2.0 Gyr). Star-forming galaxies with large reddening (*dot-dashed line in the left panel*) can reach similarly red continua in the case of very high reddening but are distinguished from the former because of the lack of any strong spectral feature in the UV, such as OB-type stars. The vertical lines (in both panels) show the three windows used for the measurement of the Mg_{UV} index (eq. [1]).

relied on their peculiar color properties. Candidates of $z \gtrsim 1.4$ passively evolving galaxies were preselected following the criteria outlined by Daddi et al. (2004a). These were calibrated on the complete K20 survey spectra database that includes the $z > 1.4$ passive and star-forming galaxies described in Cimatti et al. (2004) and Daddi et al. (2004b). Defining the color difference, $BzK \equiv (z-K)_{AB} - (B-z)_{AB}$, the candidate $z \sim 2$ passive galaxies can be located with $BzK < -0.2 \cap (z-K)_{AB} > 2.5$ (Daddi et al. 2004a).

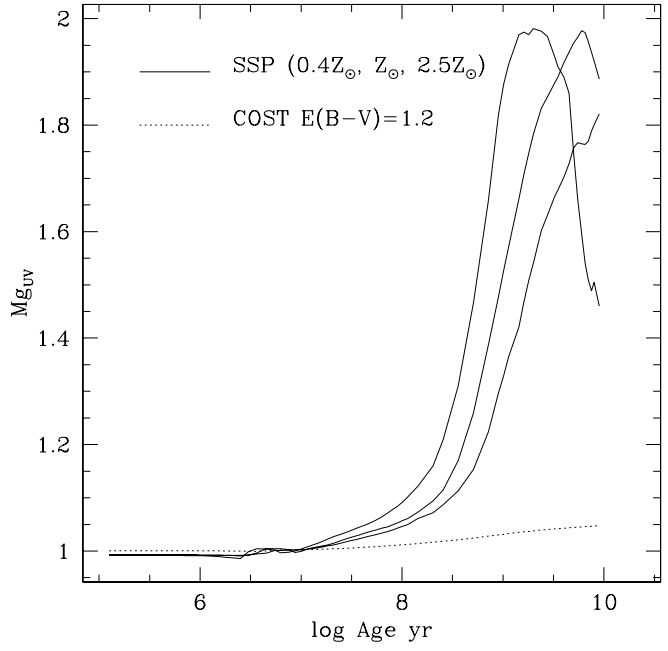

FIG. 2.—Age dependence of the Mg_{UV} index (eq. [1]). The three solid lines correspond to SSP models for three different metallicities ($0.4\,Z_\odot$, $Z_\odot$, and $2.5\,Z_\odot$; higher metallicity produces a larger Mg_{UV} index at fixed age for most of the age range). The dotted line is for a constant star formation model with $E(B-V) = 1.2$. The Mg_{UV} index is almost independent on reddening and on the resolution of the spectra for $R \gtrsim 50$, the typical rest-frame resolution of our GRAPES spectra.

Objects satisfying the above condition were retained as a primary sample. However, based on Figure 8 (*bottom left diagram*) of Daddi et al. (2004a), galaxies having $z - K > 2.5$ and $BzK > -0.2$ were also considered for detailed analysis, as young "protoellipticals" could be in principle located at $BzK > -0.2$. Moreover, despite the extreme depth of B-band UDF imaging, the errors on $B - z$ colors are found to be large for many red objects with $z - K > 2.5$.

These preselection criteria require B-, z-, and K-band imaging. We have used the deep VLT ISAAC K_s-band images[9] over the GOODS field (Fig. 3; B. Vandame et al. 2005, in preparation) and the ultradeep ACS images[10] of the UDF for the B and z bands (S. V. W. Beckwith et al. 2005, in preparation). Galaxies were selected over the area of about 12 arcmin^2 where deep ACS images are available, requiring total magnitudes $K_{AB} < 23$ as measured by SExtractor MAG_AUTO (Bertin & Arnouts 1996). This is ~1 mag fainter than the total magnitude limit of the K20 survey, while the area is a factor ~3 smaller than the K20/GOODS area that is contiguous and in part overlapping with the UDF area analyzed here (Fig. 3).

Figure 4 shows the resulting BzK diagram. In order to increase the accuracy of the color measurements, we have not attempted to reduce the ACS resolution to the much poorer 0.″5 seeing of the K-band data. For the ACS bands, we used SExtractor MAG_AUTO measured in consistent apertures defined in the z band (double-image mode). SExtractor MAG_AUTO measurements were also used for the K band (single-image mode).

[9] Available at http://www.eso.org/science/goods/releases/20040430/.
[10] Available at http://archive.stsci.edu/prepds/udf/udf_hlsp.html.

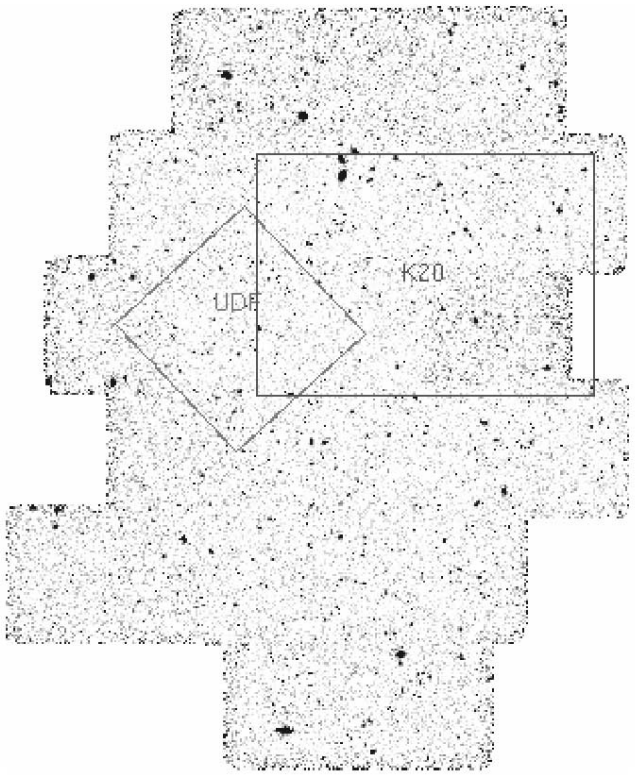

FIG. 3.—Relative layout of the UDF, K20, and GOODS-South regions. The background image is the GOODS *K*-band mosaic used in this paper. [*See the electronic edition of the Journal for a color version of this figure.*]

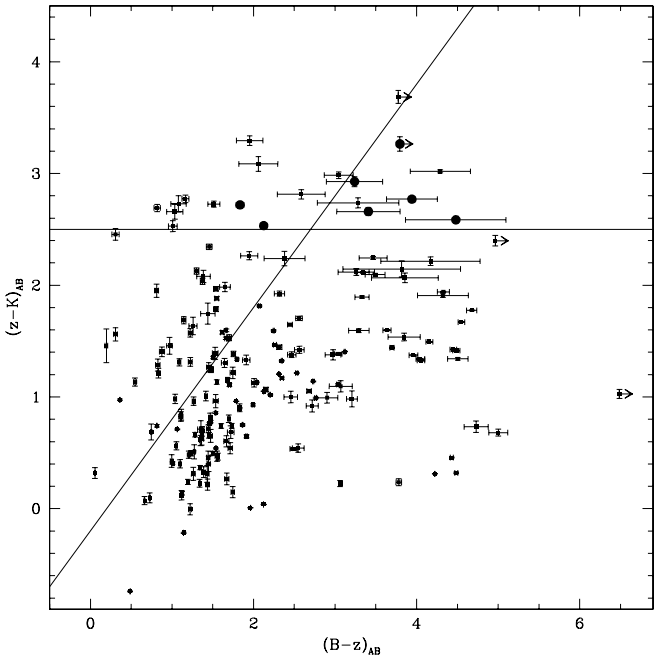

FIG. 4.—*BzK* diagram for galaxies with $K_{AB} < 23$ in the UDF. Objects with $z - K > 2.5$ were retained as possible high-*z* old galaxy candidates. The seven passive early-type galaxies with proposed redshift $1.4 \lesssim z \lesssim 2.5$ are shown by large filled circles. Five occupy the region with $BzK < -0.2$, as expected (Daddi et al. 2004a), while two bluer objects are also identified. [*See the electronic edition of the Journal for a color version of this figure.*]

This results in a different physical aperture of the magnitudes in the optical versus near-IR bands. However, we verified that the resulting $z - K$ was not biased (at least within $\sim$0.05 mag on average) with respect to seeing-matched $z - K$ magnitudes for objects in common with the catalog of Daddi et al. (2004a). There are 20 objects with $z - K > 2.5$, seven of which also have $BzK < -0.2$.

4. ANALYSIS: REDSHIFTS AND SPECTRA

To measure the redshifts of the selected candidates, we have used all the available information, including high-quality *HST* low-resolution optical spectra and the multicolor photometric data available for the UDF, as discussed in the next two sections.

4.1. *HST ACS Low-Resolution Spectroscopy*

The *HST* ACS grism G800L data, obtained as part of the GRAPES project, cover the wavelength range 5000–11,000 Å, with maximum efficiency around 7000–8000 Å. The spectral dispersion is about 40 Å pixel^{-1}. The low sky background at these wavelengths from space allows *HST* grism data to be taken in slitless mode so that all UDF objects are simultaneously observed in the GRAPES data. The effective spectral resolution depends on the spatial size of the objects. For unresolved sources the spectral dispersion translates into a resolution of $R \approx 100$ at 8000 Å, while extended sources have lower-resolution spectra. Thanks to the absence of OH sky emission lines and the exquisite spatial resolution of *HST*, the GRAPES low-resolution spectroscopy allows us to reach relatively high S/N ratios on the continuum. For compact galaxies, like those considered in this paper, one gets S/N $\sim$ 10 at 8000 Å over a 100 Å region for $i_{AB} \sim 25.5$ for the 10^5 s integration time of the GRAPES data. This is significantly better than what can be reached from the ground with red-optimized CCDs on 8–10 m class telescopes with similar integration times, except for the narrow spectral windows free of OH sky emission lines.

Full details of GRAPES grism data reduction and calibration are given in P04. As slitless spectroscopy may imply spectra superposition from neighboring sources, the data were obtained at five independent position angles to minimize this effect. Narrow extraction windows (see P04) were used to maximize the S/N ratio of the resulting spectra. The five epoch spectra were co-added, avoiding regions contaminated by neighboring objects, as described in P04.

4.2. *Spectral Analysis*

The 20 red galaxies selected as described in § 3 were inspected by looking for the Mg_{UV} feature described above and at their overall spectral shape. Some of the spectra had too low of a S/N ratio to be useful because the objects are too faint in the optical. Seven objects were retained as likely $z \gtrsim 1.4$ passive object identifications, five of which have $BzK < -0.2$. Spectra for these seven galaxies are shown in Figure 5. The five single-epoch spectra of each object were inspected to verify that the detected features were persistent and not due to obvious spurious artifacts.

In order to objectively identify the redshift of the objects, and to exclude possible feature misidentifications, we cross-correlated the spectra with galaxy templates from the Bruzual & Charlot (2003) library before definitively assigning redshifts. The model templates were convolved with the line-spread functions computed from the light profiles of the galaxies, to reproduce the actual spectral resolution of the data. Note that

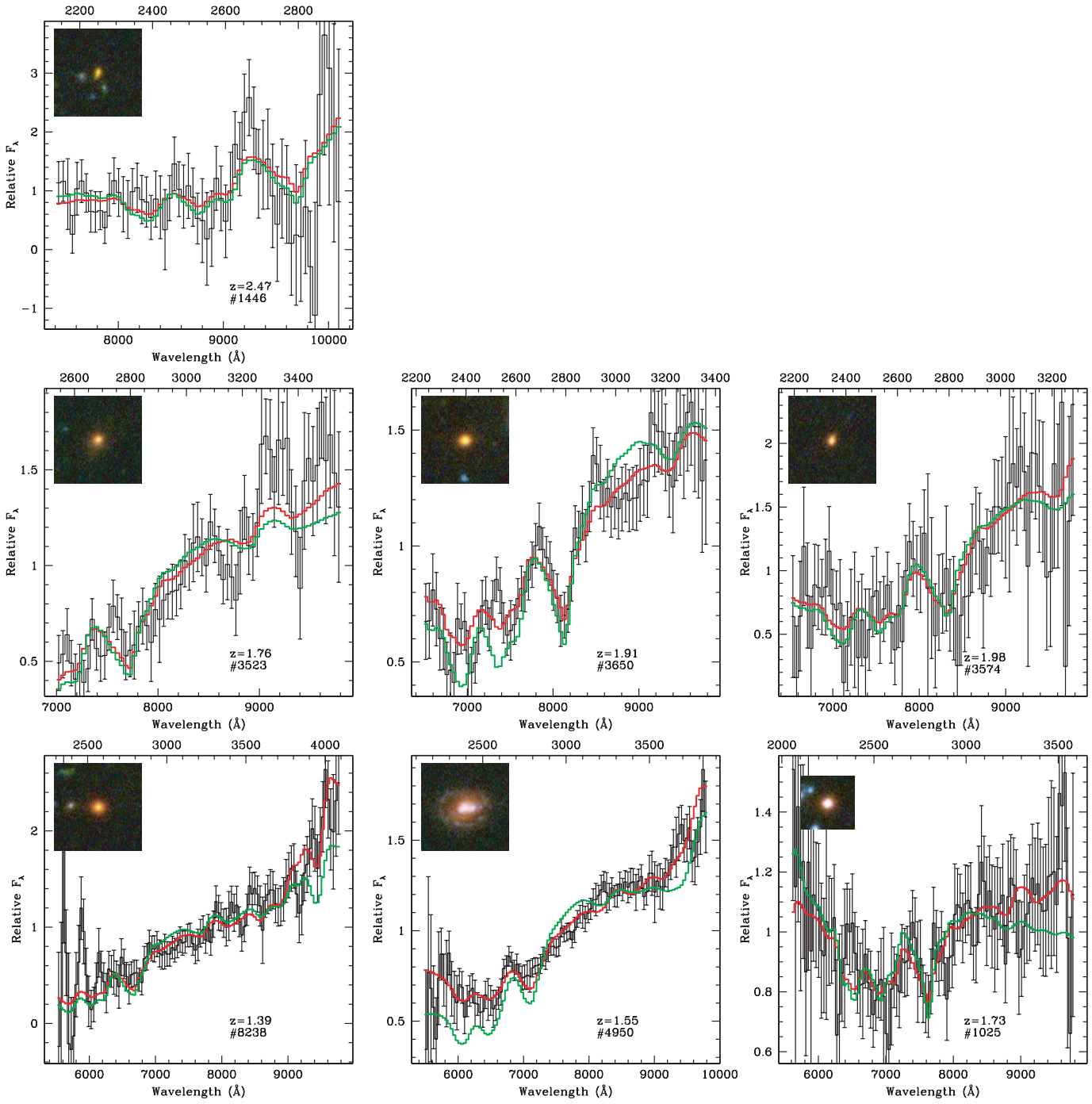

FIG. 5.—GRAPES *HST* ACS spectra of the seven passively evolving galaxies with $1.39 < z < 2.47$. In each panel the observed spectra are fitted with Bruzual & Charlot (2003) models for old galaxies (*red*) and main-sequence stars from the Kurucz library (*green*). Proposed redshifts and UDF IDs are labeled on each panel. Both rest-frame (*top x-axis*) and observed (*bottom x-axis*) wavelengths are labeled. Color inserts for each galaxy are $5'' \times 5''$ (except for No. 1025, which has a smaller color image because it is close to the edge of the UDF field).

this fitting approach is rather conservative because most of the continuum region of the spectra with no detected features has no strong effect on the fitting and reduces the impact of the regions where the actual features are; i.e., it dilutes the signal by giving equal weight to all data in the spectral range.

Two classes of models were adopted for the spectral fits in order to bracket the general cases of old and passive galaxies versus strongly dust-reddened galaxies. For old galaxies, we considered simple stellar populations (SSP) and a model with exponentially declining star formation rate (SFR) with timescale $\tau = 0.3$ Gyr. Ages less than the age of the universe at each redshift were required, and a maximum reddening of $E(B-V) < 0.2$ was allowed. We considered solar and 40% solar metallicity. For dusty galaxies we used constant SFR models with unlimited[11] dust reddening and solar metallicity.

In all seven cases, except for No. 3523, the models for old passive galaxies converge to the solution guessed by eye, with

[11] Practically, for the intrinsically bluest models, $E(B-V) \lesssim 1.5$ is more than sufficient to provide SEDs as red or redder than the data at any redshifts.

TABLE 1
PHOTOMETRIC PROPERTIES, SED, AND SPECTRAL FITTING RESULTS

			PHOTOMETRY						SED FITTING			SPECTRAL FITTING		
ID	R.A.	DECL.	z^{tot} (AB)	K^{tot} (AB)	$B-z$ (AB)	$z-K$ (AB)	$R-K$ (Vega)	$J-K$ (Vega)	z_{phot}	$\chi^2_{r,old}$	$\chi^2_{r,d}$	z_{spec}	$\chi^2_{r,old}$	$\chi^2_{r,d}$
8238.....	03 32 36.9	−27 46 28.5	23.80	21.22	4.48	2.58	6.43	2.01	1.26 ± 0.04	1.1	2.8	1.39 ± 0.01	0.59	0.61
4950.....	03 32 30.0	−27 47 26.8	22.56	19.90	2.12	2.64	5.58	1.96	1.57 ± 0.03	0.4	7.2	1.55 ± 0.01	0.83	0.79
1025.....	03 32 43.0	−27 48 45.1	24.20	21.48	1.83	2.72	5.41	1.87	1.72 ± 0.04	0.6	5.1	1.73 ± 0.01	0.40	0.54
3523.....	03 32 33.7	−27 47 51.1	24.34	21.68	3.41	2.66	5.84	1.79	1.72 ± 0.04	2.2	9.0	1.76 ± 0.02	0.70[a]	0.64
3650.....	03 32 38.1	−27 47 49.8	24.18	21.36	3.94	2.82	6.00	1.84	1.90 ± 0.03	2.2	9.7	1.91 ± 0.01	0.76	0.98
3574.....	03 32 39.1	−27 47 51.6	25.29	22.39	3.24	2.90	6.29	1.89	1.94 ± 0.04	3.0	11.3	1.98 ± 0.02	0.41	0.46
1446.....	03 32 39.2	−27 48 32.4	26.06	22.80	>3.80	3.26	5.42	3.32	2.85 ± 0.05	2.1	5.8	2.47 ± 0.02	0.58	0.71

NOTE.—IDs for UDF galaxies are those from the publicly available catalog release V1, available at ftp://udf.eso.org/archive/pub/udf/acs-wfc/h_udf_wfc_V1_cat.txt. Note that the total magnitudes were derived from Sérsic profile fitting, as described in § 5.2, and are brighter than the Kron total magnitude measured by SExtractor by ∼0.4 mag, on average. Conversion factors from Vega to AB magnitudes are −0.09, 0.22, 0.94, and 1.87 for *B*, *R*, *J*, and *K*, respectively. Photometric redshift errors are at the 68% level, as computed by *hyperz*. Spectroscopic redshift errors are the formal 68% range on the fit determined following Avni (1976) for the case of one interesting parameter (redshift), added in quadrature to systematic and random errors in the wavelength calibration, which are about 20 Å (Pasquali et al. 2003; P04) and produce an additional uncertainty of $\sigma_z \lesssim 0.01$. Units of right ascension are hours, minutes, and seconds, and units of declination are degrees, arcminutes, and arcseconds.

[a] The spectral fit for object 3523 has a slightly lower minimum for $z \sim 1.1$, a redshift that is, however, fully inconsistent with the photometric SED.

the Mg_{UV} feature correctly identified. In most cases dusty models provide a worse fit to the data; however, differences are not large, and all reduced χ^2 are below 1 and acceptable. The minima of reduced χ^2 all being below 1 might actually suggest that some significant degree of correlation (e.g., due to the reduction process; P04) is present in the data. Results of the spectral fitting are summarized in Table 1, where in all cases the z_{spec} is quoted for the best-fitting old/passive galaxy model, as justified from the results of the next section. Detailed description of redshift assignment for individual objects is described in § 4.4, following the analysis of the spectral energy distributions (SEDs) and photometric redshifts.

4.3. *SEDs and Photometric Redshifts*

To further constrain the redshift identifications, we used the extremely high quality imaging available on the UDF area. This includes the *BViz* ACS imaging and the *J* and *H* NICMOS imaging. ISAAC *J*- and *K*-band data were also used, the *J*-band filter of ISAAC being much narrower than that of NICMOS, as well as *V* and *R* from FORS2, which have central wavelengths that are quite different from those of the ACS bands. To match ground-based and *HST* data sets we proceeded as discussed in § 3. It was checked that over the common range the photometric SEDs and the *HST* low-resolution spectra were consistent. The SEDs of the seven $z > 1.4$ early-type galaxy candidates are shown in Figure 6. The same range of model parameters that was used for the spectral fitting is used in the figure, corresponding to the two classes of old/passive versus dusty models. The *hyperz* code (Bolzonella et al. 2000) was used for the model fitting and to derive photometric redshifts. A lower limit of 0.05 mag was used for the photometric errors in all the bands, in order to account for photometric zero-point uncertainties and possible residual uncertainties in the match of the different data sets.

Results of the SED fitting and photometric measurements are summarized in Table 1. SED fitting in all cases results in significantly better fits for models of old/passive galaxies with respect to those for dusty objects, rejecting dusty models at more than 3 σ confidence levels (Avni 1976) in all cases. Best fits have generally acceptable reduced χ^2 and indeed look reasonable by eye inspection. The agreement between the photometric redshifts and the spectroscopic redshifts, derived from the spectral fitting with old stellar populations, is very good, with six out of seven objects having $|z_{spec} - z_{phot}| \lesssim 0.1$.

4.4. *Redshifts, and Redshift-Quality Classes for Individual Objects*

Based on the results of SED and spectral fitting, we assigned redshifts and redshift-quality classes ("A" for good-confidence redshifts, "B" for less secure ones) for individual objects. A quality A redshift is assigned when the Mg_{UV} feature appears well detected and when the photometric and spectroscopic redshifts are in good agreement (i.e., within $\Delta z = 0.1$).

1. *No. 8238: z = 1.39, class B.*—The SED and spectral fitting agree within $\Delta z = 0.13$. The spectrum is consistent with the presence of the 4000 Å break and with the Mg_{UV} feature.

2. *No. 4950: z = 1.55, class A.*—The SED and spectral fitting agree very closely with $\Delta z = 0.02$. The spectrum clearly shows the Mg_{UV} feature. The rise toward the UV below 6000 Å is consistently present also in the photometry. This object is also part of the K20 survey (Cimatti et al. 2002b) with a measured redshift of $z = 1.553$. A weak [O II] λ3727 emission line is detected in the K20 survey spectrum.

3. *No. 1025: z = 1.73, class A.*—The SED and spectral fitting agree extremely closely with $\Delta z = 0.01$. The spectrum, which is fairly blue especially at $\lambda < 2500$ Å, shows the characteristic Mg_{UV} feature. The upturn in the blue spectra is consistent with that expected for A-type stars (Fig. 1). This source is detected in the X-rays (Giacconi et al. 2002; Alexander et al. 2003; see § 9). Zheng et al. (2004) propose $1.47 < z_{phot} < 1.58$, reasonably consistent with our spectroscopic redshift.

4. *No. 3523: z = 1.76, class B.*—The spectrum would suggest $z \sim 1.1$ as the best-fitting old galaxy solution by placing the 4000 Å break around 9000 Å, and the Ca II H and K lines in the dip at 8700 Å. The above solution is not consistent with the photometric SED, because at $z \approx 1.1$ no reasonably good fit could be obtained. A secondary solution from spectral fitting, with nearly the same χ^2 as the best one, is found at $z = 1.76$, in very good agreement with the photometric redshift within $\Delta z = 0.04$. We propose the latter solution as the spectroscopic redshift for this galaxy. The Mg_{UV} feature is not evident, although the spectrum is consistent at least with the presence of a 2900 Å break. The proposed redshift thus relies strongly on the

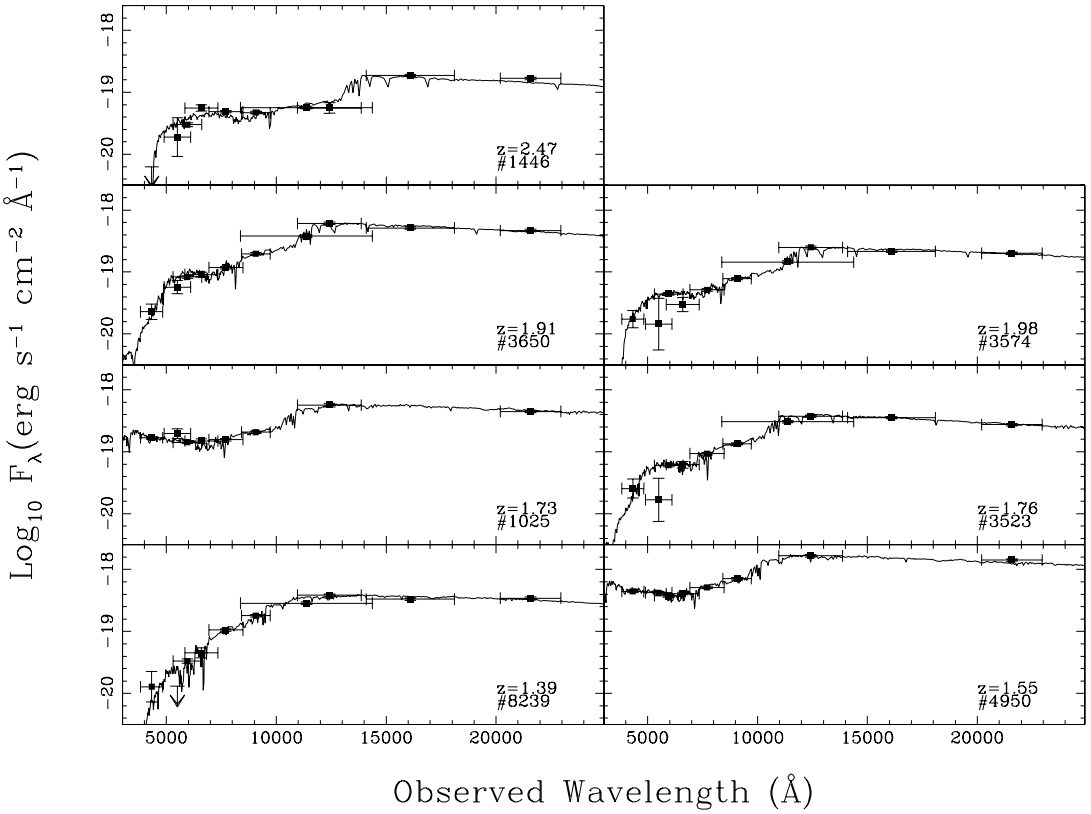

FIG. 6.—Observed SEDs of the seven $z \gtrsim 1.4$ early-type galaxies. The imaging data shown in the plot are, from blue to red: F435W, *V*, F606W, *R*, F775W, F850LP, F110W, *J*, F160W, and *K*. The best-fit Bruzual & Charlot (2003) SSP models overplotted here are consistent with those used in Fig. 5. Redshift is increasing from bottom to top. The upper limits shown are at 1 σ. [*See the electronic edition of the Journal for a color version of this figure*.]

overall SED and spectral fitting. The absorption-like spectral features at 8900 and 9200 Å are to be considered spurious noise features for our proposed redshift. Yan et al. (2004a) suggest that this is an old galaxy at $z_{\rm phot} = 1.6$, in good agreement with the redshift proposed here.

5. *No. 3650: z = 1.91, class A*.—The SED and spectral fitting agree extremely closely with $\Delta z = 0.01$. The Mg_{UV} feature is very evident.

6. *No. 3574: z = 1.98, class A*.—The SED and spectral fitting agree closely with $\Delta z = 0.04$. The spectrum shows the Mg_{UV} feature. Yan et al. (2004a) propose that this is an old galaxy at $z_{\rm phot} = 1.9$, in excellent agreement with our spectroscopic redshift.

7. *No. 1446: z = 2.47, class B*.—The SED and spectral fitting are in fair agreement with $\Delta z \sim 0.4$. The spectrum has a strong feature at 9200 Å that in the spectral fitting with old models is identified with the Mg_{UV} feature. Emission line identification algorithms described in Xu et al. (2005), however, pick up the feature as a possible emission line. If the feature is an emission line we find best-fitting $\lambda \sim 9230$ Å, FWHM ~ 160 Å, and EW $\sim$ 150 Å. The large FWHM and EW would suggest an AGN emission line. This would be possible, as the object is a hard X-ray source (Giacconi et al. 2002; Alexander et al. 2003), although no strong emission line is detected in the FORS spectra described by Szokoly et al. (2004). We tried to fit its photometric SED with reddened QSO AGN templates, but the fit still significantly prefers old/passive models. As the SED drops in the *B* band, the only plausible AGN line identification would be [C III] λ1909 at $z = 3.83$, with the Lyman break producing the *B*-band drop. Zheng et al. (2004) propose a photometric redshift $4.13 < z_{\rm phot} < 4.35$, which is not far from that. For $z = 3.83$ one would expect to detect an even stronger C IV λ1550 emission at about 7500 Å, which instead is not present. For $z = 3.83$ it would also be difficult to explain the overall shape of the SED with, e.g., the break between the *J* and *H* bands. Chen & Marzke (2004) propose that this object is a dusty galaxy with $z_{\rm phot} =$ 3.43, which is not consistent with our analysis, while Yan et al. (2004a) propose that this is an old galaxy at $z_{\rm phot} = 2.8$.

The spectral and photometric properties show that we can distinguish two classes of objects among our sources. Objects 4950 and 1025 have in fact significant *B*-band excess flux with respect to the others (see Figs. 4 and 8), suggesting the presence of hotter stars. These two objects are discussed in more detail in § 6.2.

4.5. *Discussion of Redshift Identifications*

The proposed redshifts are based on low-resolution spectra that, we recall, do not allow us to detect individual absorption or emission lines, as is ordinarily done for redshift identifications of faint-galaxy spectroscopy. Therefore, we cannot exclude with full confidence the possibility that, in a minority of the cases, our identifications might be somehow mistaken. We believe, however, that identifications are generally reliable because (1) the spectral fitting routine generally converges to the solution guessed by visual inspection of the spectra when using templates for passive galaxies, (2) the photometric redshift estimated with the high-quality UDF data are in very good agreement with the proposed spectroscopic redshifts with median $|z_{\rm spec} - z_{\rm phot}| = 0.04$ only, and (3) there is an overall consistent picture as signatures of old stellar populations are seen in the spectra, the SEDs strongly suggest passive stellar

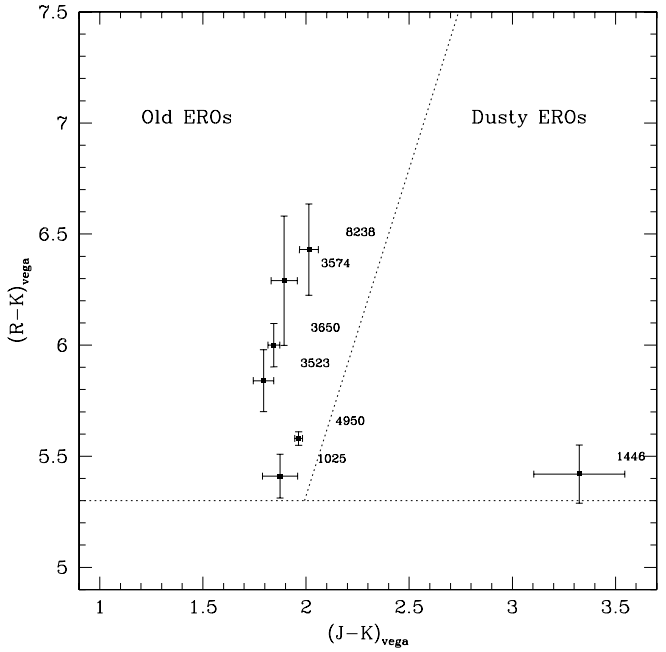

FIG. 7.—Pozzetti & Mannucci (2000) diagnostic diagram with the $R - K$ vs. $J - K$ colors of our sample galaxies. The dotted lines show the $R - K > 5.3$ limit of validity of the criterion, and the division between old and dusty star-forming EROs for $z \lesssim 2$.

populations, and morphologies of early-type galaxies are recovered, as discussed in § 4.6.

As an additional test (Fig. 7), we verified the location of the seven sources in the Pozzetti & Mannucci (2000) diagram. The $R - J$ versus $J - K$ colors of the sources are consistent with those expected for passively evolving galaxies up to $z \lesssim 2$. The only exception is object 1446, with much redder $J - K$ color and proposed $z = 2.47$, a redshift at which the above diagnostic may not apply. We verified that using the criterion proposed by Pozzetti & Mannucci (2000) for $z > 2$, involving the J, H, and K bands, object 1446 would also be classified as a passive red galaxy. We also verified, for further overall consistency, that best-fitting models of the SEDs produce good fits to the *HST* grism spectra.

4.6. *Sample Completeness*

The completeness of the $z \gtrsim 1.4$ sample of passive galaxies was investigated. We checked whether additional passive $z \gtrsim 1.4$ galaxies could be found among bluer objects with $2.2 < z - K < 2.5$. It may be expected that toward the lowest $z \sim 1.4$ range of redshifts, some early-type galaxy could have $z - K < 2.5$ (either intrinsically or because of the errors in the photometry). No convincing case could be found. Among the remaining unidentified galaxies with $z - K > 2.5$ there are three more objects with compact morphology that are not in our sample with proposed spectroscopic redshift. One of these is object 869, which is a $z = 3.064$ type 2 QSO (Szokoly et al. 2004) with no distinctive feature in our GRAPES spectrum. The other two are UDF 8363 and 5056, which have noisy spectra with no feature identifiable and photometric redshifts 2.30 and 1.43, respectively. These might be additional passive $z > 1.4$ objects. Their *BzK* colors are consistent with the $BzK < -0.2$ region (object 8363 is the reddest one in $z - K$ with a lower limit to $B - z$; Fig. 4).

There are 10 more galaxies with $z - K > 2.5$ that remain unidentified in GRAPES spectra and have irregular, diffuse, and sometimes merging-like morphologies, reminiscent of the $z \sim 2$ star-forming galaxies (also having similar colors and magnitudes) shown in Daddi et al. (2004a, 2004b). Only one of these formally has $BzK < -0.2$. The fact that we cannot detect features of old stars in these objects could be an observational bias, as the S/N of the spectra for these extended and diffuse galaxies is generally low. However, they might be more likely genuine dust-reddened star-forming galaxies. An analysis of the stacked X-ray and radio emission of galaxies with similarly $z - K$ colors and having $BzK < -0.2$ in the K20 survey suggests that these objects are mainly vigorous dust-reddened starbursts at $z > 1.4$ (Daddi et al. 2004a, 2004b).

In summary, there are at most only two reasonable additional candidates for passive $z > 1.4$ galaxies that are compact and have the expected *BzK* colors. These are less luminous than those for which we propose a spectroscopic redshift. Additional passive objects might still be present among the galaxies with irregular morphology, although no object with similar properties is currently known both at high and lower redshift.

4.7. *Redshift Clustering*

We mention, in passing, the slight evidence of redshift clustering that can be drawn from the redshifts of our sample. For these objects, the correlation length r_0 might be comparable to or even higher than that for typical EROs at $z \sim 1$ ($r_0 \sim 10\ h^{-1}$ Mpc; Daddi et al. 2001; McCarthy et al. 2001; Brown et al. 2005), as these could truly be the first collapsed massive galaxies. This should translate into significant pairings between our sample and other galaxies, e.g., to those in the K20 region (Fig. 3). In fact, the $z = 1.91$ galaxy is at the same redshift of the Cimatti et al. (2004) $z = 1.903$ elliptical and is also at the same redshift as that of the $z = 1.901$ near-IR bright galaxy in Daddi et al. (2004a). The $z = 1.73$ and 1.76 galaxies in our sample may actually be at the same redshift given the errors, presumably $z = 1.73$, where two other near-IR bright massive star-forming galaxies also lie (Daddi et al. 2004a). Also, at $z = 1.55$ and $z = 1.39$ other massive star-forming galaxies are found in the K20 survey. Similarly, three out of four of the $z > 1.5$ early-type galaxies of Cimatti et al. (2004) are at $z \sim 1.61$, and strong pairing is also observed in the McCarthy et al. (2004) sample.

5. ANALYSIS: MORPHOLOGY

We inspected by eye the morphological appearance of the seven galaxies with proposed spectroscopic confirmation as old high-z stellar populations. Figure 8 shows the available *HST* imaging (see also the color images of the objects in Fig. 5). All objects look very compact and regular. Object 4950 appears to be a bulge-dominated nearly face-on spiral, i.e., an Sa, with perhaps evidence of merging or cannibalism in the blue bands. Object 1446 is the most elongated and might be an early spiral or an S0 galaxy. The other objects are visually classified as E/S0 systems. In order to provide a more quantitative estimate of the morphology, we used CAS (concentration, asymmetry, and clumpiness) and Sérsic profile fitting.

5.1. *CAS Analysis*

The concentration and asymmetry of all the galaxies having $z - K > 2.5$ were measured in the i band, corresponding to about 3000 Å rest frame for $z \sim 2$ (similar results were obtained in the z band). Parameter definitions consistent with those given in Conselice (2003) were used. Figure 9 shows the resulting measurements. Objects with proposed spectroscopic

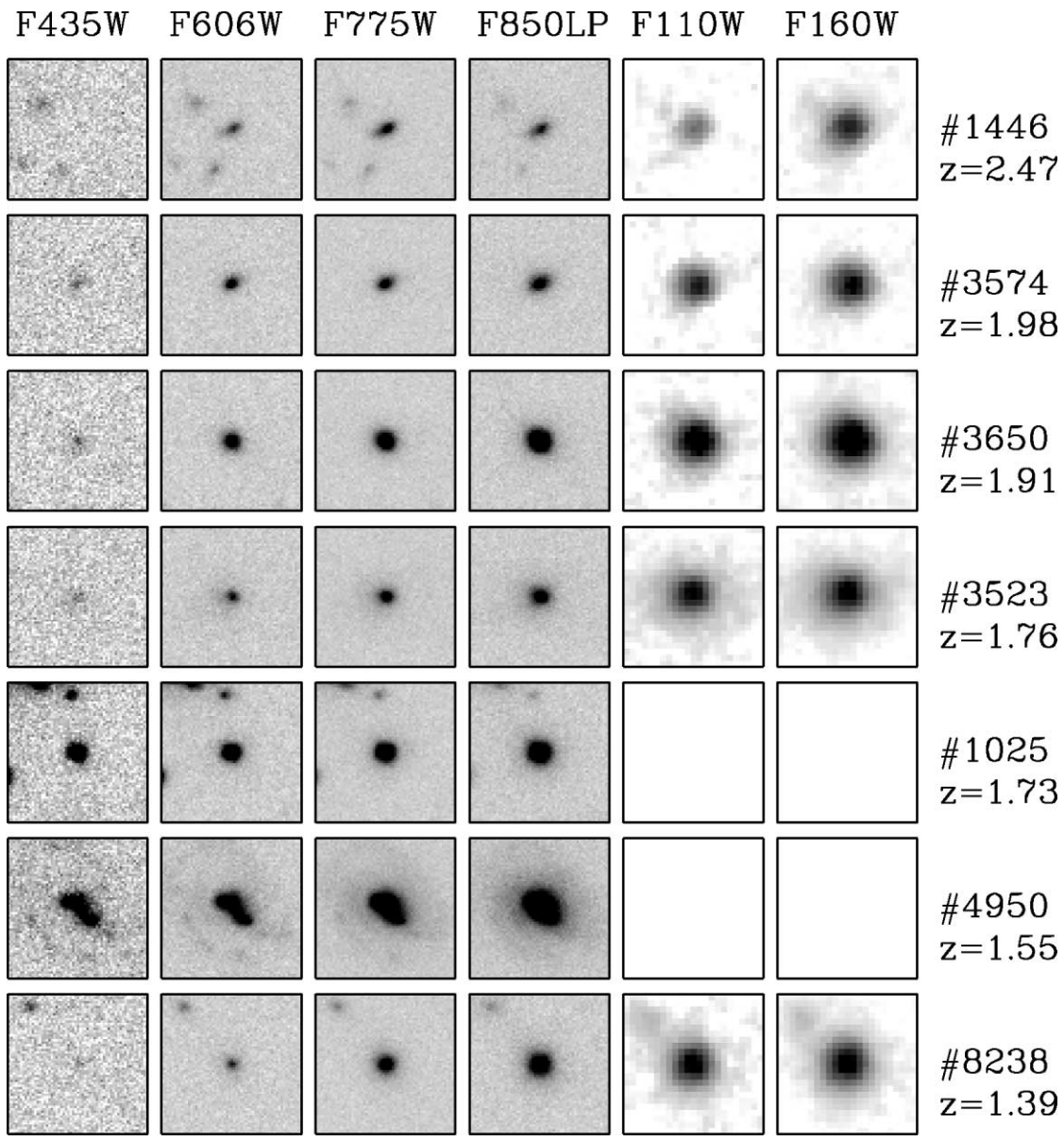

FIG. 8.—Multiband *HST* imaging of the high-z early-type galaxies. Each image is 2″ on a side. Within the ACS imaging, as within the NICMOS imaging but on a different scale, the same range of fluxes (f_λ) are plotted in a logarithmic scale, to provide direct comparison with Fig. 6 and among different objects or different bands. The F435W band appears the noisiest in f_λ, where, however, only object No. 1446 is not significantly detected. The NICMOS images show in some cases the extended, low-surface-brightness wings of the steep de Vaucouleurs–like profiles. Object Nos. 1025 and 4950 are outside of the region covered by the NICMOS imaging.

confirmation as $z > 1.4$ passive galaxies tend to have high concentrations and low asymmetry (see also Table 2). In general, these objects occupy a range of values consistent with those of early-type galaxies; for example, all have concentrations $C > 2.6$, a value marking the boundary between early- and late-type galaxies in the local universe (Strateva et al. 2001; see also Conselice 2003). The asymmetries are generally low: $\lesssim 0.2$ in all cases.

5.2. *Sérsic Profile Fitting*

We used GALFIT (Peng et al. 2002) to model the light profile of the seven objects with proposed redshift confirmation. Both i- and z-band analyses were performed for a cross-check of the results and to test for possible color trends. The point-spread function (PSF) was derived for each band by averaging stellar objects in the field (Pirzkal et al. 2005). All the $z \gtrsim 1.4$ passive galaxies are resolved. We fitted Sérsic (1968) profiles of the form

$$\mu(r) = \mu_e e^{-\kappa\left[(r/r_e)^{1/n}-1\right]}, \quad (2)$$

where r_e is the effective radius, μ_e is the effective surface brightness, n is the free Sérsic index, and κ is determined from n in order for half of the integrated flux to be within r_e. Results are summarized in Table 2. The Sérsic profile fitting also allowed us to derive the total magnitudes, as listed in Table 1. The quoted uncertainties are purely statistical and derived by GALFIT on the basis of the image noise. Notice that the errors on the parameters are correlated. For example, fitting with a larger n generally implies larger r_e and brighter total magnitudes.

The Sérsic index n is generally found to be consistent within the estimated noise between the i and z bands. Derived values

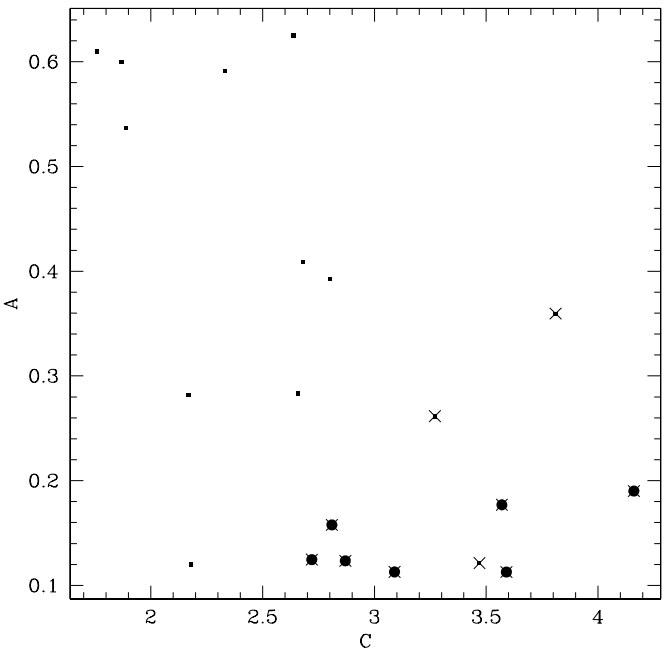

FIG. 9.—Concentration vs. asymmetry parameters in the *i* band for the 20 galaxies with $z - K > 2.5$ and $K_{AB} < 23$ in the UDF. Large circles are for the seven $z \gtrsim 1.4$ early-type galaxies. A cross through a symbol denotes an object classified as "compact" by visual inspection, as opposed to the remaining objects (shown without crosses) that are classified as "irregular/merger." The three compact objects that are not in our list of passively evolving galaxies are described in more detail in § 4.6. [*See the electronic edition of the Journal for a color version of this figure.*]

are in the range of 2.8–2.9, with many of them close to the de Vaucouleurs value of $n = 4$, typical of E/S0 systems, with the exception of the object with the highest estimated redshift (No. 1446) having $n \approx 1$, which is consistent with the presence of an exponential disk and may be an early-type spiral or perhaps an S0 galaxy. This galaxy is reminiscent of the $z = 2.5$ evolved disk galaxy discussed by Stockton et al. (2004). For object 4950 the Sérsic fit leaves strong residuals, corresponding to the features visible in the *B* band (see Fig. 8). Nevertheless, the *z*-band light appears to be dominated by a regular spheroid with $n \sim 4$. A fit in the *i* band was not attempted for this object.

The effective radii in the *i* and *z* bands are also in most cases consistent, suggesting the lack of strong color gradients within the galaxies. Some of the typical effective radii are very small, of order $r_e \sim 2$–4 ACS UDF pixels, corresponding to 0.″06–0.″12 for the 0.″03 pixel^{-1} scale of the drizzled UDF images or to a physical size $\lesssim$1 kpc (proper length). We come back to these issues in § 8. The axial ratios b/a are also consistent between the two bands, generally quite close to unity and consistent with the range expected for E/S0 systems.

The proposed redshift identifications result in a reasonably complete (see § 4.6), magnitude-limited sample of $z > 1.4$ galaxies representative of old-star dominated, morphologically established early-type galaxies. These high-redshift spheroids appear to be already dynamically relaxed, with the possible exception of object 4950.

6. RESULTS: STELLAR POPULATIONS OF $z > 1.4$ EARLY-TYPE GALAXIES

In order to derive the characteristic stellar population properties of the seven $z > 1.4$ galaxies, we compared the photometric SEDs (with deep imaging data in 10 bands from *B* to *K*, as described in § 4.3; see also Fig. 6) to stellar population synthesis models from the Bruzual & Charlot (2003) library, at the (fixed) spectroscopic redshift of each source. We base our physical parameter estimates mainly on the photometric SEDs rather than on the spectra, because of the much wider wavelength range spanned by the former. In particular we would expect the rest-frame UV photometry, including the very deep *B*-band images, to strongly constrain the presence or lack thereof of young stellar populations. The near-IR bands provide instead a census of the past star formation.

A more extended library than the one adopted in § 4.3 was used in this case, including models with 0.2, 0.4, 1.0, and 2.5 solar metallicity. Reddening is restricted to $E(B - V) < 0.2$ (we use a Calzetti et al. 2000 law). Some small amounts of dust reddening are also sometimes found among local early-type galaxies (see, e.g., Goudfrooij & de Jong 1995) and could be more often present at these high redshifts, as we are observing closer to the star formation epoch. For the star formation history we adopted SSP models and exponentially decreasing models with $\tau = 0.1$, 0.3, and 1.0 Gyr. In addition, we considered models with step-wise star formation history, with constant SFR lasting for 0.1, 0.3, 1, and 2 Gyr, followed by a period of passive evolution. Only ages less than the age of our universe at the fitting redshifts were allowed. The parameters we are mainly interested in are the age and stellar mass of the galaxies, and we determined 95% ranges for these two parameters, following Avni (1976) and marginalizing over $E(B - V)$, metallicity, and SFR history (Table 3). We also fitted main-sequence star templates from the Kurucz library to the *HST* spectra of all galaxies (Fig. 5). The Mg_{UV} indexes were measured. Indeed, in most cases they are significantly larger than 1, as expected for old stellar populations.

All the results are shown in Table 3. Best fits at the spectroscopic redshifts are shown for all objects in Figure 6. The

TABLE 2
MORPHOLOGICAL PARAMETERS

		i BAND		*z* BAND				*i* BAND			
ID	TYPE	*C*	*A*	*n*	r_e (pixel)	r_e (kpc)	*b*/*a*	*n*	r_e (pixel)	r_e (kpc)	*b*/*a*
8238.....	E/S0	3.09	0.11	8.2 ± 1.5	11 ± 4.7	2.8 ± 1.2	0.89	5.8 ± 1.0	4.7 ± 1.1	1.2 ± 0.3	0.88
4950.....	Sa+M?	3.57	0.18	4.3 ± 0.4	22 ± 3.7	5.6 ± 0.9	0.60	...	...	...	0.88
1025.....	E/S0	3.59	0.12	4.2 ± 0.5	2.9 ± 0.3	0.74 ± 0.1	0.85	5.0 ± 0.7	2.1 ± 0.3	0.54 ± 0.1	0.85
3523.....	E/S0	4.16	0.19	9.0 ± 1.6	11 ± 4.3	2.8 ± 1.1	0.74	9.7 ± 2.0	16 ± 8.0	4.0 ± 2.0	0.71
3650.....	E/S0	2.87	0.12	4.7 ± 0.6	3.1 ± 0.3	0.79 ± 0.08	0.74	5.4 ± 0.8	3.2 ± 0.5	0.81 ± 0.13	0.72
3574.....	E/S0	2.72	0.12	2.9 ± 0.3	2.5 ± 0.2	0.63 ± 0.05	0.45	2.8 ± 0.4	2.4 ± 0.4	0.61 ± 0.1	0.39
1446.....	S0/Sa	2.81	0.16	0.8 ± 0.2	3.1 ± 0.5	0.76 ± 0.12	0.35	1.4 ± 0.3	3.9 ± 0.8	0.96 ± 0.20	0.26

TABLE 3
STELLAR POPULATION PROPERTIES

ID	z_{spec}	Class	$\chi^2_{r,m}$	$P(\chi^2_{r,m})$ (%)	M_B (Vega)	$U-B_{rest}$ (Vega)	$B-V_{rest}$ (Vega)	M_* (10^{11} $M_\odot$)	M_*/L_B ($\odot$)	Age_{pass} (Gyr)	z_{pass}	S_{type}	Mg_{UV}
8238.....	1.39	B	1.5	13	−20.98	0.23	0.91	1.0–2.4	2.5–6.2	0.5–4.5	>1.6	F5	1.14 ± 0.19
4950.....	1.55	A	1.2	30	−22.86	0.19	0.76	2.9–7.3	1.3–3.4	0.6–2.5	1.8–3.7	F0	1.17 ± 0.04
1025.....	1.73	A	0.7	68	−21.76	0.19	0.76	1.0–1.8	1.3–2.2	0.6–1.2	2.1–2.6	A3	1.14 ± 0.06
3523.....	1.76	B	1.7	8.4	−21.73	0.20	0.67	1.0–1.5	1.3–1.8	0.5–1.2	2.1–2.6	F2	0.94 ± 0.09
3650.....	1.91	A	1.7	7.8	−22.32	0.20	0.67	1.3–2.0	1.0–1.5	0.6–1.6	2.3–3.4	F0	1.25 ± 0.05
3574.....	1.98	A	2.8	0.2	−21.41	0.16	0.68	0.5–0.9	0.9–1.6	0.5–1.2	2.3–2.9	F0	1.5 ± 0.2
1446.....	2.47	B	10	0	−21.62	0.20	0.59	0.7–1.1	1.0–1.7	0.3–0.7	2.8–3.2	F5	2.8 ± 0.6

NOTE.—$\chi^2_{r,m}$ is the reduced χ^2 of the best fit. Ranges for M_* and Age_{pass} (and thus for M_*/L_B and z_{pass}) are given at the 95% confidence level. $U-B$ and $B-V$ colors are derived from the best-fitting model.

reduced χ^2_m are generally low, with large associated probabilities, and the best fits to the photometric SEDs (Fig. 6) look generally very good. An exception is object 1446, with large χ^2_m at the tentative spectroscopic redshift $z = 2.47$. Still, its SED looks reasonably well reproduced from eye inspection (Fig. 6). In part, the bad χ^2_m may be due to the presence of AGN continuum emission starting to contribute to the near-IR bands' fluxes.

The derived masses are generally large, in the range 0.5–7.3×10^{11} $M_\odot$. Notice that these values were derived using the total flux of these galaxies estimated from Sérsic profile fittings. The use of Kron magnitudes derived by SExtractor would have implied an underestimation of the masses by ∼40% on average. Absolute magnitudes and colors were derived for our targets by using the best-fitting models for computing *K*-corrections. The derived *B*-band rest-frame stellar mass-to-light ratios are typically about 1–2 in solar units, as compared to the dynamically estimated total (thus including the contribution of dark matter) mass-to-light ratios of up to 6 for local early-type galaxies (van der Marel 1991). Accounting for the fact that the adopted Salpeter IMF all the way down to 0.1 $M_\odot$ may be overestimating the stellar masses (and mass-to-light ratios) by at least 30%, and that dust reddening in the fit can affect by up to 1 mag the *B*-band rest frame, this is consistent with a dimming of a few magnitudes from passive evolution to $z = 0$, as computed from aging the best-fitting Bruzual & Charlot models. The inferred stellar mass-to-light ratios at $z = 1.4$–2 also appear to be consistent with the trend established for cluster early-type galaxies up to $z \sim 1.3$ on the basis of fundamental plane studies (van Dokkum et al. 2004; Renzini 2005). The 95% ranges on fitted properties are not very narrow in most cases. Availability of *Spitzer* photometry providing access to the near-IR rest frame could allow us to further improve these estimates. However, the uncertainties about the importance and modeling of asymptotic giant branch (AGB) stars' contribution at those wavelengths (Maraston 2005) could further complicate the issue, our sample being perhaps the ideal one to verify the predictions of different models. A future publication will address these points.

6.1. *Formation and Ages of $z \gtrsim 1.4$ Early-Type Galaxies*

In order to characterize the evolutionary status of these objects, we estimated the quantity Age_{pass} as the time elapsed since the onset of the passive evolution (i.e., since the end of the last major burst of star formation). This is defined as the difference between the model age and the duration of the star formation phase, assumed to be equal to τ for exponential star formation (SF) histories, zero for SSP models, and the actual duration of the burst for truncated star formation models. Table 3 shows that Age_{pass} estimates are typically in the range of 0.5–1.5 Gyr, suggesting that the onset of passive evolution started at $z_{pass} \sim 2$–3.5 in most cases.

It is interesting to investigate what types of SF histories yield acceptable fits to the SEDs, as this could constrain the SF timescales in early-type galaxies. By limiting our focus to the five objects with no *B*-band excess flux, we find that the SSP and $\tau = 0.1$ Gyr models provide much better fits to the SEDs than models with $\tau = 0.3$ or 1 Gyr. Exponentially declining star formation histories with $\tau \geq 0.3$ Gyr are clearly inappropriate for these objects, as they strongly overproduce the rest-frame UV fluxes. A similar result was found by McCarthy et al. (2004) and may seem to imply relatively short formation timescales (e.g., less than 0.3 Gyr). This appears to be consistent with the α-enhancement found to be typical of elliptical galaxies at $z = 0$, which also suggests short formation timescales (see, e.g., Thomas et al. 2002, 2005). However, the failure of models with $\tau \geq 0.3$ Gyr may not be due to their long formation timescales but to the exponentially declining tail of star formation. Physical reasons, such as the feedback from supernova explosions or from the onset of AGN activity (Granato et al. 2004), suggest that in more physically motivated models the SF might be completely stopped by such feedback. The "truncated" models that we considered allow us to explore this possibility and check whether much longer SF timescales are consistent with our data. In fact, these truncated models produce acceptable fits to the SEDs even for the case of 2 Gyr lasting star formation. In conclusion, the available portion of the SED and the presence of the Mg_{UV} feature allow us to set strong constraints on Age_{pass} but not on the previous duration of the SF activity. Rest-frame near-IR data from *Spitzer* could also help constrain this latter quantity.

The fits with $\tau = 0.1$ Gyr models allow us to derive limits to the maximum amount of ongoing SFR in these passive galaxies, as these models have some residual SF at any time. For the five objects, one gets residual SFR $\lesssim 0.1$ $M_\odot$ yr^{-1} with the $\tau = 0.1$ Gyr models. Even if continuing at this level for a full Hubble time to $z = 0$, this would increase the galaxies' masses by less than 1%. Of course, we neglect here the possibility of completely dust-extincted SF, which we would not detect anyway in the optical–IR.

Further constraint on the formation processes of early-type galaxies can be obtained from the comparison with theoretical simulations. For example Hernandez & Lee (2004) estimated the relaxation timescales of elliptical galaxies formed as the result of the merger of two equal-size disks and the Press-Schechter probability of such a merger happening in practice.

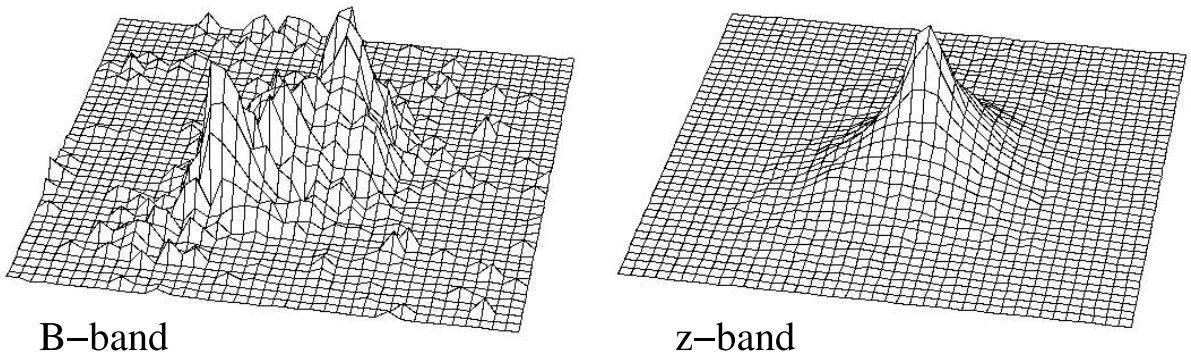

FIG. 10.—Comparison of the surface brightness distribution for object 4950 in the *B* and *z* bands. The same range of fluxes (f_λ) are plotted for the two objects. The peak of the *z*-band image corresponds to a relative dip in the *B* band, which is instead dominated by two blobs separated by $\sim$1 kpc ($0''.1$) from the galaxy center. The *z*-band surface brightness profile clearly shows the central cusp and extended wings typical of de Vaucouleurs galaxies. Neither the faint spiral arms nor ring are visible in these images. See also Fig. 8 and the color inset in Fig. 5 for comparison.

For early-type galaxies with stellar masses similar to those that we derive, i.e., $M_* \sim 10^{11}\ M_\odot$, they suggest that if such objects are found at $z \gtrsim 1.6$, as we do, it is highly unlikely that they have formed through mergers of equal-size spirals.

6.2. *Blue Excess Early-Type Galaxies*

We now come back to the two objects with *B*-band flux excess, Nos. 4950 and 1025. It is perhaps surprising that $\mathrm{Age_{pass}}$ measurements for these two objects are not distinguishable from those of the other, redder galaxies. However, unlike for the other five galaxies, these two bluest early-type objects can only be fitted by the $\tau = 0.3$ Gyr models, which seem to produce the correct balance between old and younger stars. The residual SFRs of the best-fitting $\tau = 0.3$ Gyr models is 5–10 $M_\odot\ \mathrm{yr}^{-1}$ for No. 4950 and about half of that for No. 1025. This is also revealed for No. 4950 by the detection of a weak [O II] λ3727 emission in the K20 survey spectrum.

These two objects have $BzK > -0.2$ because of their relatively blue $B - z$ color (see Fig. 4). Passively evolving galaxies shortly after the quenching of SF are expected to show similar colors (Daddi et al. 2004a), but on the other hand the blue $B - z$ colors may also be due to a secondary burst of star formation, involving a small fraction of the total stellar mass.

This is most likely the case for galaxy 4950. Its morphology changes strongly from the *B* band to the *z* band (Figs. 8 and 10). The *B*-band light is fairly irregular, with a significant substructure of 3–4 blobs. It is unlikely that such a clumpy structure is a bar, as these are typically more regular. The blobs visible in the *B* band may be instead due to an ongoing merger or cannibalism of smaller galaxies or satellites. The *z*-band light distribution is instead more regular and appears typical of a spheroid. A feature looking like spiral arms or perhaps a ring is also detected at a distance of about 5 kpc from the center, which is significantly less luminous than the central light in both *B* and *z* bands. From the spectrum we find additional evidence for composite stellar populations. The best stellar template fit is in fact an F0, but best fits with A5 and F2 stars are found when limiting the fit to below or above a 2800 Å rest frame, respectively. The *B*-bright clumps may have been formed or accreted after the *z*-band spheroid was in place.

The morphology of object 1025 is instead regular from the *B* band to the *z* band, with no obvious changes. Sérsic profile fits were obtained for this object also in the *V* and *B* bands, and we found that it is consistent with a high Sérsic index, $n \sim 4$, in all ACS bands. There is instead a trend of decreasing effective radius with decreasing wavelength that appears significant, possibly due to the presence of a color gradient (§ 8). In the *HST* grism spectrum we find that no change is detected when fitting templates of stars below or above a 2800 Å rest frame only, and an A3-type star spectrum dominates the light consistently in the $2000 < \lambda < 3600$ Å range. There is therefore no strong evidence in this object for the coexistence of two clearly distinct stellar populations, although the fact that a simple SSP model cannot reproduce its SED implies at least a somewhat extended SF timescale. This object appears to be an early-type galaxy observed very close to some significant star formation event, when early A-type stars (rather than F-type stars found in all the other passive objects) were still dominating its UV SED. Broadhurst & Bouwens (2000) discussed the observational lack of known early-type galaxies with A-type dominated stellar populations, our object being perhaps the first known case. The relatively short lifetime of A-type stars, of order of a few hundred Myr at most, may be the actual reason why these objects are rare.

The recent star formation event may actually be the one when most of the stars in this spheroid were formed. Object 1025 would then represent the closest known link between passively evolving F star dominated early-type galaxies and the as yet not established nature of the main formation event. The relaxed morphology at this early stage would imply a fairly short dynamical relaxation timescale. If the star formation event is a secondary one, involving only a fraction of the mass, this object might instead be similar to the E+A galaxies found at lower redshift (Dressler & Gunn 1983). This single object in the $1.4 < z < 2$ redshift range corresponds, however, to a volume density that is 2 to 3 orders of magnitude higher than the local density of E+A galaxies above similar luminosities (Quintero et al. 2004). The fraction of E+A galaxies in the present sample (one out of seven) would also be higher than the mere 1% that is found locally (Quintero et al. 2004).

7. RESULTS: EVIDENCE FOR A DECLINING NUMBER DENSITY OF EARLY-TYPE GALAXIES AT $z \gtrsim 1.4$

An important question to address is how the abundance of $z \gtrsim 1.4$ passive early-type galaxies compares to the local value and to the populations of star-forming galaxies at the same redshifts. As the majority of our sample galaxies, and all of those of class "A," are located at $z < 2$, we first consider the $1.39 < z < 2.00$ redshift range for this comparison. Over the

12.2 arcmin^2 selection area this redshift range includes a volume of $\sim$20,000 Mpc^3. Summing up the galaxy stellar masses estimated in § 6, we obtain a total stellar mass in the range of 7×10^{11}–16×10^{11} $M_\odot$, and a stellar mass density in the range of 3.4×10^7–8.1×10^7 $M_\odot$ Mpc^{-3} for an average redshift $\langle z\rangle = 1.7$. The six early-type galaxies with $1.39 < z < 2.00$ correspond to a number density of 3.4×10^{-4} Mpc^{-3}.

7.1. *Evolution from $z \sim 2$ to $z = 0$*

The masses of these six galaxies are all close to or larger than 10^{11} $M_\odot$, and we can assume our sample to be reasonably complete above such a mass threshold for passive early-type galaxies down to $K_{AB} = 23$. In the local universe, the number density and the stellar mass density of passively evolving galaxies with $M_* > 10^{11}$ $M_\odot$ are about 9×10^{-4} Mpc^{-3} and 1.3×10^8 $M_\odot$ Mpc^{-3}, respectively (Baldry et al. 2004).[12] Thus our sample of early-type galaxies in $1.39 < z < 2.00$ accounts, at face value, for $\sim$35% of the number density of $M_* > 10^{11}$ $M_\odot$ passive galaxies in the local universe, and for a fraction of $\sim$25%–60% of the relative stellar mass density. Notice that at $z = 0$ about 75% of all $M_* > 10^{11}$ $M_\odot$ galaxies are classified as passive early-type galaxies (Baldry et al. 2004). We therefore infer at $z = 1.7$ a decrease in the number density of massive early-type galaxies by at most a factor of 3, if limiting to $z < 2$. The inferred fractions would be further divided by a factor of 2 if using all the volume in $1.39 < z < 2.47$.

A major limit of these calculations is represented by cosmic variance because of the small volume probed by Hubble UDF. All our passive galaxies are EROs with $R - K > 5.3$ (Table 1), which are strongly clustered populations (Daddi et al. 2000a; McCarthy et al. 2001). Clustering can produce strong fluctuations in the number density of objects over small volumes, which most likely result in an underestimate of the true densities as averaged over large volumes (Daddi et al. 2000a). If one assumes that these $z > 1.4$ galaxies have the correlation length of EROs, i.e., $r_0 \sim 10\ h^{-1}$ Mpc (Daddi et al. 2001, 2003), one finds that even at the 1 σ level the true number density (and thus the stellar mass density) of passive galaxies could be within half and twice that estimated from our sample, or between 20% and 80% of the local value.

It is clear that similar searches on much larger and independent areas would be important to measure the number density evolution with some reasonable accuracy. The UDF data set is likely to remain unique in its depth and quality for many years to come, but our result confirms that reliable estimates on the abundance of $z > 1.4$ passive early-type galaxies might be obtained by using the *BzK* photometric criteria only (Fig. 4; Daddi et al. 2004a), even without complete spectroscopic follow-up. In fact, in the UDF the sky density of the brightest ($K_{Vega} < 20$) candidate $z > 1.4$ early-type galaxies satisfying conditions $z - K > 2.5$ and $BzK < -0.2$ is not much smaller than that found in a $\gtrsim$30 times wider field survey (Kong et al. 2005). So, the densities derived over the UDF field should not dramatically underestimate the true values.

7.2. *Passive Objects at Even Higher Redshifts?*

The highest redshift passive object that we recover is at $z = 2.47$, although with "B" class redshift, while all the others lie at $z < 2$. Therefore, it is important to ask whether the paucity of $z > 2$ passive galaxies is due to the limiting magnitude of the sample (i.e., they exist but are fainter) or to passive galaxies getting rarer and rarer. Indeed, some of the galaxies in our sample are consistent with having started pure passive evolution only at $z \lesssim 2$.

We have used a V/V_{max} test to try to shed light on the issue. For each of our objects we compute the maximum redshifts at which it would still be part of the sample (i.e., with $K_{AB} < 23$, Kron magnitudes, and $z - K > 2.5$). We use the best-fitting Bruzual & Charlot models to compute *K*-corrections, and $z = 1.39$ as the lower redshift boundary. The result is that the six objects would still be in the sample at least up to $z = 3.3$ (when No. 8238 would drop out) and up to $z = 4.6$ (when, finally, No. 3650 would also drop out). With $\langle V/V_{max}\rangle = 0.14 \pm 0.04$ and a maximum $V/V_{max} = 0.35$ for No. 1446, a uniform V/V_{max} distribution is rejected at the 99.7% level, based on a Kolmogorov-Smirnov test.

There is therefore strong evidence for evolution, especially beyond $z = 2$. This means that if galaxies with masses and SEDs (i.e., ages) similar to those we see at $\langle z\rangle = 1.7$ were present at higher redshifts, we would have detected them out to $z \sim 4$ (and with $z - K > 2.5$). These results underscore a rapid disappearance of truly passive systems at redshifts $z \gtrsim 2$. This does not mean that massive galaxies were not present at earlier epochs, but rather, if existing, they were most likely still actively star forming. Notice that at $z = 4$ our universe is already $\sim$1.6 Gyr old, and in principle there would have been time to produce passively evolving galaxies with ages similar to those we see at $1.4 < z < 2.5$.

Of course, clustering can also bias this $\langle V/V_{max}\rangle$ test. For example, by chance the UDF may lack a cluster-like structure with many similar galaxies at $z > 2$ or 3. On the other hand, a similar $\langle V/V_{max}\rangle$ test in the sky-contiguous K20 survey region suggests that the *K*-band luminous *BzK*-selected starburst galaxies are evolving positively in number over the same redshift range (Daddi et al. 2004a). These *BzK* starbursts are massive (stellar masses $\sim10^{11}$ $M_\odot$), and plausible candidates for being precursors to early-type galaxies. Therefore it appears that while the number density of passive galaxies is dropping with increasing *z*, the number density of their immediate likely precursors is somewhat increasing, as expected. It is worth emphasizing that these two $\langle V/V_{max}\rangle$ tests were performed basically on the same sky area, and therefore they should be affected by clustering in a similar way.

7.3. *The Fraction of $z > 1.4$ Stellar Mass in Passive Objects*

It is interesting to estimate what fraction of the mass, or of the most massive galaxies, is in passive galaxies at the probed redshifts $1.4 < z < 2.5$. Galaxies with $BzK > -0.2$ are in most cases star-forming objects at $1.4 < z < 2.5$ (Daddi et al. 2004a), thus spanning the same redshift range of the detected passive galaxies. We can thus simply compare the sample of $BzK > -0.2$ galaxies selected to $K_{AB} = 23$ to the current sample of passive objects to the same limiting magnitude. We used the (SED-fit–based) *K*-band magnitude versus stellar mass relation calibrated in Daddi et al. (2004a). For the passive galaxies in our sample this relation provides fairly good estimates of the stellar masses, fully consistent with those listed in Table 3. As star-forming galaxies in $1.4 < z < 2.5$ we consider all $BzK > -0.2$ sources, i.e., 43 objects when excluding the two passive "blue" objects and any source with X-ray detection as likely an AGN. Of these, six have estimated stellar mass $M_* \gtrsim 10^{11}$ $M_\odot$, producing a total stellar mass of the order of 5×10^{11} $M_\odot$, or up to 10×10^{11} $M_\odot$ for those above an estimated stellar mass

[12] We account for the fact that our pure Salpeter IMF gives stellar masses at least 30% larger than those derived from the IMF used in Baldry et al. (2004).

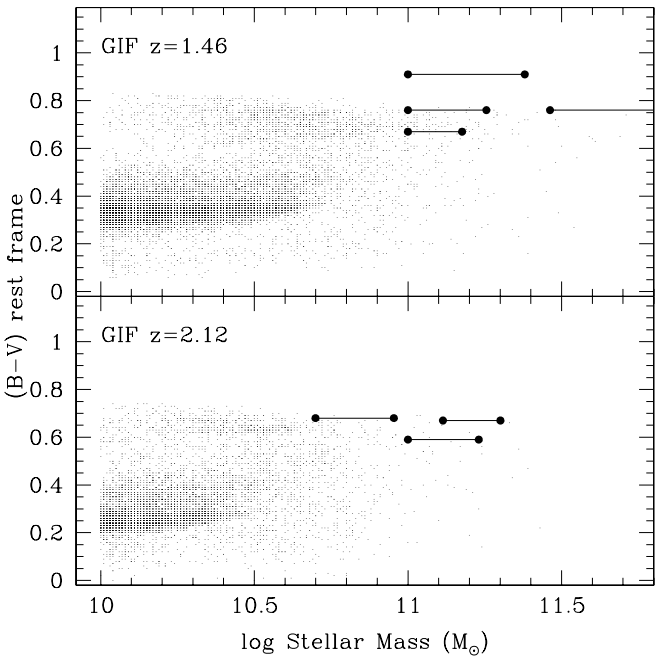

FIG. 11.—Predicted stellar masses vs. rest-frame ($B - V$) colors of galaxies from the ΛCDM simulations (Kauffmann et al. 1999). The connected filled circles are for our objects, where minimum and maximum stellar masses are shown. The early-type galaxies at $z < 1.8$ are plotted over the $z = 1.46$ simulation, while those at $z > 1.8$ are plotted over the $z = 2.12$ simulation. The volume of each simulation is 200 times larger than the UDF for $1.4 < z < 2.5$. [*See the electronic edition of the Journal for a color version of this figure.*]

limit of $M_* > 0.5 \times 10^{11}\ M_\odot$.[13] These figures are similar to those derived above for passive objects in the same redshift and mass ranges. This supports earlier hints that at $1.4 < z < 2.0$ roughly ≈50% of the stellar mass is in passively evolving galaxies, and roughly ≈50% is in vigorous star-forming galaxies, for objects with stellar masses $M_* \gtrsim 10^{11}\ M_\odot$ (Cimatti et al. 2004; McCarthy et al. 2004). By summing together the similar stellar mass density contributions from passive and star-forming galaxies at $1.4 < z < 2$ having $M_* \gtrsim 10^{11}\ M_\odot$, one gets fairly close to the local value from the SDSS (Baldry et al. 2004). However, the uncertainties due to small-number statistics and clustering and in the estimates of stellar masses are both at least a factor of ∼2. The evolution of most massive galaxies is not easily detectable up to $z = 2$, and therefore it is arguably not very strong.

7.4. *Comparison to ΛCDM Theoretical Predictions*

McCarthy et al. (2004) and Cimatti et al. (2004) already pointed out that the existence of $z > 1.4$ passive early-type galaxies in such relatively high number is at odds with current predictions of semianalytic models of galaxy formation and evolution, which suggest the passive evolution phase to be established much later, if ever. This is similar to the reported failure to account for ERO number counts, even at $z \sim 1$ (see, e.g., Daddi et al. 2000b; Firth et al. 2002). These conclusions are also supported by the current findings.

For example, among the *early* semianalytic models, the simulations[14] by Kauffmann et al. (1999) predict a number density at $z = 1.46$ of galaxies with $(B - V)_{\rm rest} > 0.6$ (Table 3) and stellar mass $M_* > 10^{11}\ M_\odot$, which is about a factor of 10 lower than recovered here in the UDF, and by $z \sim 2$ such objects should have virtually disappeared. Nevertheless, it is interesting that these models do predict that at least some galaxies exist with the colors and masses of those we observe (Fig. 11), and that a hint for a bimodal color distribution is already in place in the models at these redshifts. On the other hand, there appear to be too few massive galaxies in these simulations, either passive or star forming (Daddi et al. 2004a, 2004b; Fontana et al. 2004). Among the more recent generation of models, those by Somerville et al. (2004) are quite successful in predicting the number density of massive galaxies at high redshift but fail to produce the bimodal color distribution even at low redshift. Similarly, the hydrodynamical simulations of Nagamine et al. (2005a, 2005b) appear to match the statistic of $z = 2$ massive galaxies but are less successful in reproducing the abundance of $z \sim 2$ old and passive galaxies. There is now general agreement that one of the problems with the models is their tendency to sustain star formation in massive dark matter halos all the way to low redshifts, and intense theoretical efforts are currently under way in the attempt to cope with these discrepancies. A strong AGN feedback appears to be a viable way of switching off star formation in massive galaxies at $z \gtrsim 2$ (see, e.g., Granato et al. 2004).

8. RESULTS: MORPHOLOGY EVOLUTION OF EARLY-TYPE GALAXIES TO $z > 1.4$

The morphological properties of our sample of $z > 1.4$ passive early-type galaxies were compared to those of the corresponding local populations. Figure 12 shows the *B*-band rest-frame Kormendy (1977) relation for our objects compared to a local

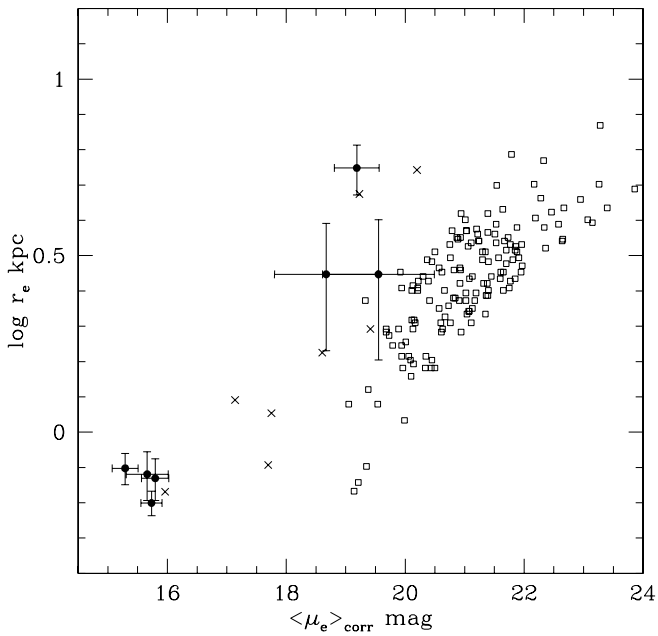

FIG. 12.—*B*-band rest-frame Kormendy (1977) relation for the $1.4 < z < 2.5$ early-type galaxies (*filled circles with error bars*), compared to Coma early-type galaxies taken from Jorgensen et al. (1995) converted to the *B* band (*squares*) and to $0.7 < z < 1.2$ early-type galaxies from the K20 survey (*crosses*; from S. di Serego Alighieri et al. 2005, in preparation). Observed values for our objects are derived from the *z*-band measurements. The average effective brightness $\langle \mu_e \rangle$ was corrected for cosmological surface brightness dimming and bandpass shift (observed *z* band to rest *B* band), but not for the (relatively uncertain) passive evolution dimming to $z = 0$. [*See the electronic edition of the Journal for a color version of this figure.*]

[13] The stellar masses estimated for the SF galaxy candidates at $1.4 < z < 2.5$ are not based on magnitudes obtained from surface brightness profile fitting, as they are for the passive galaxies, and may thus still be somewhat underestimated.

[14] See http://www.mpa-garching.mpg.de/GIF/.

sample of early-type galaxies in the Coma Cluster (Jorgensen et al. 1995) and to a sample of massive $z \sim 1$ early-type galaxies from the K20 survey (S. di Serego Alighieri et al. 2005, in preparation). The average effective surface brightness $\langle \mu_e \rangle$ (see, e.g., Ziegler et al. 1999 for its definition) has been corrected to $z = 0$ accounting for the $(1 + z)^4$ cosmological surface brightness dimming. A color term was applied to transform our z-band measurements to rest-frame B band, and similarly the Jorgensen et al. (1995) r-band measurements were corrected using $B - r = 1.15$ (Ziegler et al. 1999). When not accounting for the expected dimming of the B-band rest frame due to the aging of the stellar populations, the $z > 1.4$ objects are largely offset from the local Kormendy relation (Fig. 12). The expected dimming to $z = 0$ can be computed on the basis of the inferred best-fitting Bruzual & Charlot (2003) models, although with large uncertainties given to the range of acceptable best-fitting parameters (especially ages and SF histories). Typically, a dimming by a few magnitudes is derived, and these large passive evolution corrections, albeit uncertain, would bring the seven passive $z > 1.4$ galaxies in reasonable agreement with the local Kormendy relation.

We notice, however, that four out of the seven objects have very small effective radii, $r_e < 1$ kpc, and passive evolution would bring them in a region of the r_e-μ_e diagram where very few local galaxies are found. Moreover, local galaxies with $r_e < 1$ kpc tend to be much less massive than our $z > 1.4$ objects. Similarly, the stellar surface mass density μ_* of the four galaxies, defined as $\mu_* = M_*/(2r_e^2)$, is more than a factor $\sim$10 higher than that of local galaxies with similar stellar masses (Kauffmann et al. 2004). All in all, the $z > 1.4 r_e < 1$ kpc objects cannot be the progenitors of the $z = 0$, low-mass galaxies with similar effective radii.

Similarly, about half of $z \sim 1$ massive early-type galaxies from the K20 survey, shown in Figure 12, have sizes of about 1 kpc that are smaller than their local massive counterparts. Small sizes of K20 early-type galaxies were also inferred by Cassata et al. (2005) for the higher-redshift sample of four early-type galaxies at $z > 1.5$, i.e., $r_e = 1$–3 kpc, measured on ACS z-band data, as in this work. Waddington et al. (2002) showed that their two $z \sim 1.5$ radio-selected early-type galaxies have sizes that are too small (3 kpc), as compared to lower-redshift samples. Stanford et al. (2004) present a rest-frame B-band morphological analysis of early-type galaxies to $z = 1.4$ in the Hubble Deep Field–North, based on *HST* NICMOS, showing indeed a trend of significantly smaller sizes of luminous galaxies with respect to local massive counterparts (see their Fig. 16). An analogous result might be noticed in Figure 4 of Gebhardt et al. (2003).

Therefore, it appears well established observationally that some fraction of high-redshift passive early-type galaxies appear significantly smaller then their likely $z = 0$ descendants. While this is similar to the well-known trend of size reduction with redshift for star-forming galaxies (see, e.g., Ferguson et al. 2004), this effect had not been highlighted and/or discussed previously for early-type galaxies if not for the two radio galaxies of Waddington et al. (2002). It is somehow surprising because one would expect that these massive galaxies, which are already undergoing passive evolution, should evolve smoothly into local massive ellipticals with no major change in their properties if not for aging of the stellar populations. The availability of the ultradeep UDF imaging might allow us to better constrain and understand this issue.

We tried to investigate the possible reasons for this effect on our sample of $z > 1.4$ early-type galaxies. The small effective radii we derive with the Sérsic fitting might be due to the presence of an unresolved nuclear component, e.g., from an AGN. Actually, two of the four objects with small r_e are detected in X-rays (see § 9). For the two compact objects with the highest S/N ratio in the z-band imaging (Nos. 1025 and 3650) we attempted to fit their surface brightness profiles with two component models, Sérsic plus a pointlike source. The resulting best fit is still dominated by the Sérsic component, but its r_e is not significantly increased with respect to the single-component fits; only a lower Sérsic index n is derived. However, when forcing r_e to be large, a good fit with $r_e \simeq$ few kpc can be obtained consistently with the local objects and still have large n values. In this case the nuclear source is about 2 mag fainter than the spheroid, in agreement with the fact that the optical SEDs and spectra appear dominated by stellar light (§§ 4 and 6). If this is the reason for the small radii, it would imply a widespread nuclear activity, or relics of nuclear starbursts, in $z \sim 1.4$–2 early-type galaxies. Close inspection of the inner regions of local early-type galaxies does in fact reveal the presence of faint nuclear point sources in nearly 50% of the cases (Ravindranath et al. 2001). These nuclear sources might have been significantly more luminous/frequent at high redshifts.

If instead the small r_e values are not (or not always) due to the presence of nuclear emission, two possibilities may help to solve the puzzle and reach consistency with the local galaxy populations: either a strong morphological K-correction or the physical sizes will increase with time. Larger sizes at $z = 0$ would move the galaxies roughly along the Kormendy relation by decreasing the average effective surface brightness and would bring our objects' positions in Figure 12 into better agreement with local ones.

A possible mechanism for size evolution is substantial satellite engulfment by the massive red galaxies as they evolve to lower redshifts, which would imply an additional growth of their stellar mass. Object 4950 might be an example of this process in action. Confirmation of this scenario would require the detection of large concentrations of satellite galaxies in the vicinity of the passive $z > 1.4$ galaxies. This option might be tested in the future by using the *ultradeep* UDF data.

In relation to the morphological K-correction option, we note that blue cores are not yet uncommon among $0.5 < z < 1$ ellipticals (Menanteau et al. 2001, 2004) and that the observed z band corresponds to 2600–3800 Å in the rest frame for $1.4 < z < 2.5$ (so somewhat bluer than the 4300 Å of the B band). The most direct way to check this option would be to obtain Sérsic profile fits in the NICMOS F110W and F160W bands, bracketing the rest-frame B band for $1.4 < z < 2.5$. However, this is technically difficult, mainly because of the large 0.″2 pixel size of NICMOS (a factor of 4 larger than the ACS pixels) corresponding to $\sim$2 kpc at $z \sim 2$. Attempting such fits is beyond the scope of the present work. What we checked instead was the trend of r_e with wavelength, within the range covered by the ACS data. We constructed $i - z$ color maps of all our $z > 1.4$ galaxies (Fig. 13), but among the four objects with $r_e < 1$ kpc, only No. 1025 shows a quite prominent blue core. This object also exhibits a strong trend of r_e with wavelength, as shown in Figure 14, while a Sérsic profile consistent with $n \sim 4$ is found in all the ACS bands. An extrapolation would give r_e larger by 50% in the rest-frame B band with respect to that measured in the observed z band. Still, this increase would not suffice to bring this object at $z = 0$ on the populated part of the Kormendy relation, as that would require an increase by a factor $\sim$3. Yet, we cannot currently rule out the possibility that r_e may change more steeply with wavelength, especially beyond the 4000 Å

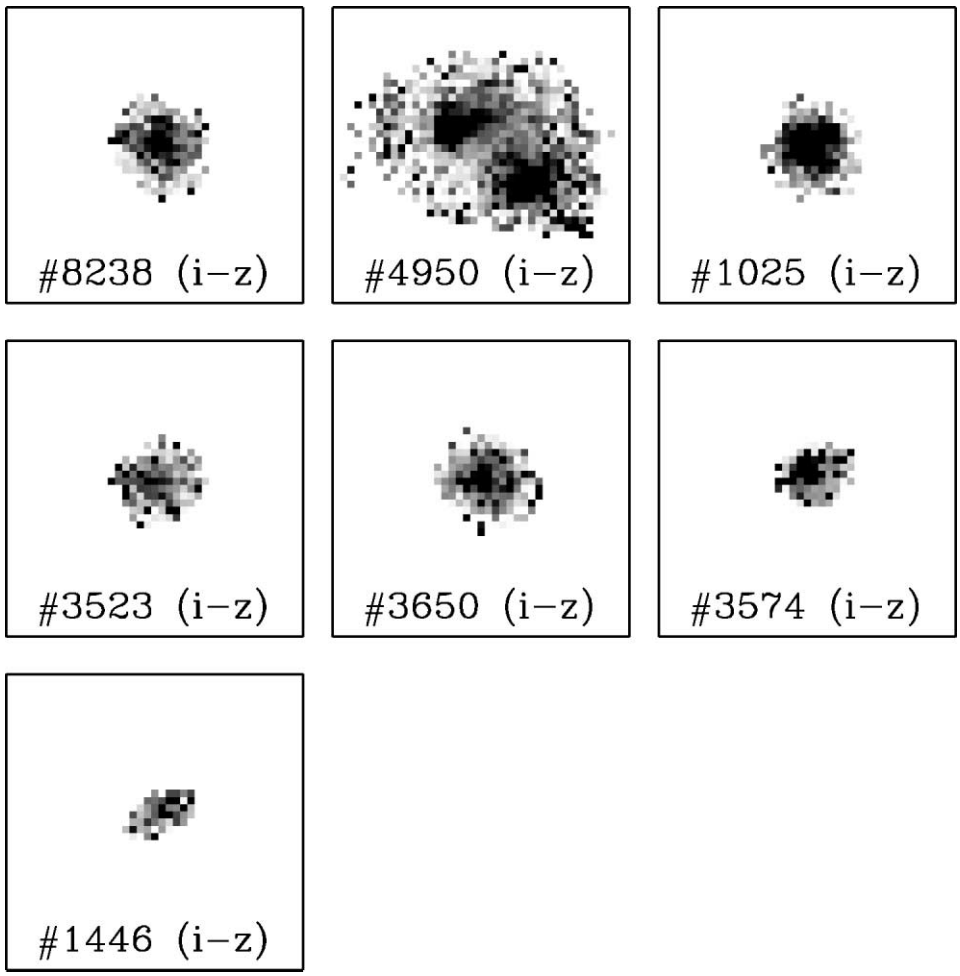

FIG. 13.—$(i - z)$ color maps; darker regions correspond to bluer $i - z$ colors. Only pixels with S/N > 3 in both i and z bands were considered. No attempt was made to account for the different PSF between the two bands; thus, the bluer (i.e., darker in the images) cores of most objects are likely the result of PSF differences. Obvious exceptions are object 4950, where two blue blobs are clearly visible, and 1025, which shows a strong color gradient and blue core.

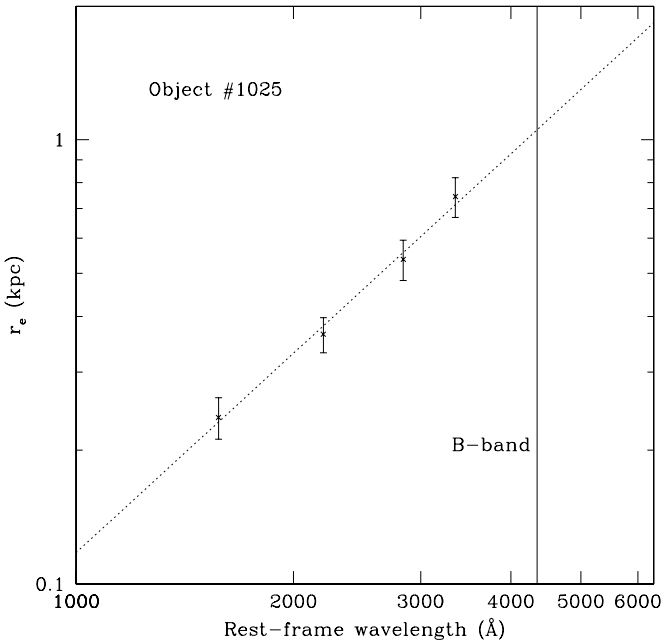

FIG. 14.—Dependence of the effective radius on wavelength for object 1025 at $z = 1.73$. The observed trend would imply r_e about 50% larger at rest-frame B band (4350 Å) with respect to observed z band (or rest frame 3350 Å), but still ~1 kpc only.

break. We finally note that small r_e values in the rest-frame B band are common among early-type galaxies to $z = 1.4$ (Stanford et al. 2004), which outlines the existence of this problem also when using B-band rest-frame measurements. A final assessment of why some high-z ellipticals have such small effective radii and how they relate to local E/S0 galaxies is left to future investigations.

9. RESULTS: THE X-RAY PROPERTIES OF $z > 1.4$ EARLY-TYPE GALAXIES

Two of the seven $z > 1.4$ early-type galaxies discussed here are detected in the 1 Ms *Chandra* X-ray observations (Giacconi et al. 2002), and their properties are reported in Table 4. The two sources are both very hard (HR > 0.4), and both of them were discussed by Padovani et al. (2004) as possible QSO 2 candidates.[15]

Object 1446 is close to the detection limit with ~20 net counts, almost all from the hard band (HR > 0.42), and we estimate its luminosity to be $L_{2-10\,\mathrm{keV}} = 2.2 \times 10^{43}$ ergs s^{-1}. Object 1025 is detected with ~90 net counts, thus allowing a rough spectral analysis. Figure 15 shows the X-ray spectrum of the object along with an absorbed power law at the source

[15] The luminosities derived by Padovani et al. (2004) are larger than those inferred here, given that these authors put these objects at slightly higher redshifts.

TABLE 4
X-Ray Emission Properties

ID	ID (G02)	ID (A03)	z	$F_{\rm soft}$ (cgs)	$F_{\rm hard}$ (cgs)	$N_{\rm H}$ ($\rm cm^{-2}$)	$L_{2-10\ \rm keV}$ (cgs)	X/O	X/K
1025.....	256	255	1.73	0.9×10^{-16}	4.1×10^{-15}	$\sim 5 \times 10^{23}$	8×10^{43}	12	2.5
1446.....	605	243	2.47	$<0.4 \times 10^{-16}$	4.6×10^{-16}	(HR > 0.42)	2×10^{43}	5	1

redshift. The best-fitting rest-frame column density is $N_{\rm H} = 5 \times 10^{23}$ $\rm cm^{-2}$, and the corresponding unabsorbed X-ray luminosity is $L_{2-10\,\rm keV} = 8 \times 10^{43}$ ergs $\rm s^{-1}$. Given the high column density and the X-ray luminosity close to 10^{44} ergs $\rm s^{-1}$, this object can be classified as an X-ray QSO 2. It is intriguing that the optical spectrum appears to be dominated by stellar light, which may imply that the obscuring torus is also blocking most of the emission in the optical and near-IR domains. An excess emission with respect to the power-law continuum is present at $\sim$2.3–2.4 keV. This would be consistent with the presence of a redshifted 6.4 keV Fe Kα emission line. Indeed, when a Gaussian line is added to the model spectrum, the fit improves and suggests a redshift $z = 1.71$, in excellent agreement with the redshift measured in the optical/near-IR, and a rest-frame line equivalent width of $\sim$350 eV, similar to that found in obscured X-ray sources (see, e.g., Brusa et al. 2005b; Maccacaro et al. 2004).

Both sources have large X-ray to optical flux ratios (X/O). Coupled with the analysis of Mignoli et al. (2004), which suggests that most of the hosts of hard X-ray AGN with large X/O and $R - K > 5$ are spheroids at $z > 1$, this implies a close connection between hard X-ray sources and high-redshift early-type galaxies.

Although based on two objects only, the fraction of AGNs at $z \sim 2$ in these early-type galaxies is at face value $\sim$30%. This is larger than that observed for the early-type sample of $z \sim 1$ EROs discussed by Brusa et al. (2002; no X-ray emission was revealed in a sample of eight sources) and much larger than the $\sim$1% value observed locally. This is similar to the fraction of AGNs among EROs at the probed K magnitudes (Alexander et al. 2003; Brusa et al. 2005a), underlining again the possible close connection between the formation of AGNs and early-type galaxies.

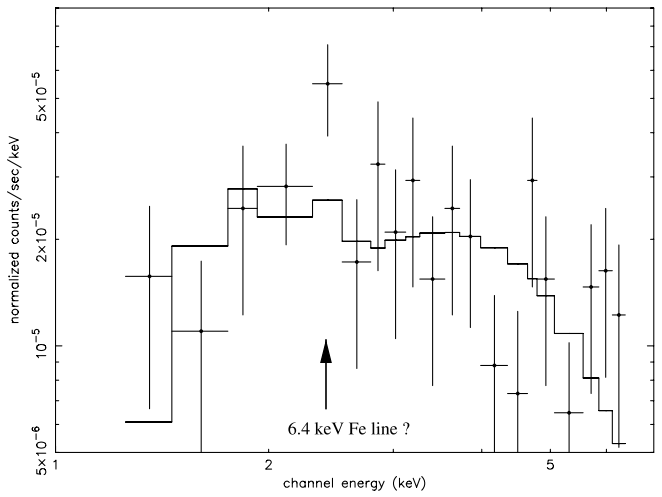

Fig. 15.—X-ray spectrum of No. 1025 from *Chandra*, fitted with a $\Gamma = 2.0$ power law and absorbing column density of $N_{\rm H} = 5 \times 10^{23}$ $\rm cm^{-2}$. The excess flux at 2.4 keV is consistent with the 6.4 keV Fe line, redshifted at $z = 1.73$. The presence of such a strong Fe emission is reasonable (Brusa et al. 2005b), given the very hard X-ray spectrum and high absorption column density of the source.

10. SUMMARY AND CONCLUSIONS

Based on the *BzK* two-color selection criterion meant to identify $z > 1.4$ passively evolving galaxies, a sample of seven objects has been identified in the UDF for which ACS grism spectra confirm both the high redshift ($1.4 \lesssim z \lesssim 2.5$) and the current absence of (or very low) ongoing star formation. The analysis conducted over the *ultradeep* ACS imaging further shows that the objects are morphologically early-type galaxies.

The redshifts are derived from the identification of the spectral feature at the rest frame $2640 < \lambda < 2850$ Å due mainly to Mg I and Mg II absorptions in late A- and F-type stars, and which shows up prominently only in synthetic stellar populations with no (or very low) star formation in the last $\sim$0.5 Gyr. The SEDs and ACS grism spectra of five of the objects are best reproduced by a star formation history initiated $\gtrsim$1.5 Gyr before and completely discontinued over the last $\sim$0.5–1.5 Gyr, implying that the passive evolution started at $z \simeq 2$–3.5. In the other cases a similar age constraint is inferred, but the spectra are best reproduced by an exponentially declining SFR, with $\tau \sim 0.3$ Gyr.

The overall SEDs of the objects indicate stellar masses in excess of $\sim 10^{11}$ $M_\odot$, and we infer that the co-moving volume density of such massive, early-type galaxies at $\langle z \rangle \simeq 1.7$ is about one-third of the local value. The uncertainty in the derived fraction is dominated by cosmic variance, given the small field covered by the UDF. Allowing for the expected clustering of these galaxies, we infer that at the 1 σ level such a fraction could be as low as $\sim$20% or as high as $\sim$80%. Clearly, the exploration of wider fields is necessary to accurately pinpoint the actual decrease with redshifts of the number density of massive galaxies that are passively evolving. However, a $V/V_{\rm max}$ test indicates that beyond $z \sim 2$ this number density is likely to drop very rapidly.

One intriguing aspect of the present findings is the quite small effective radii derived from the ACS z-band images, which in four out of seven cases are less than 1 kpc. Given their high mass, the passive evolution of such very compact objects will bring them in a region of the Kormendy relation (or, equivalently, of the fundamental plane) that is depopulated at $z = 0$. We discuss various possibilities to explain this apparent paradox, including a morphological K-correction (e.g., due to the possible presence of blue cores in these galaxies), an AGN pointlike source biasing the r_e measurements, or eventually some evolutionary effects, such as if the observed galaxies were still subject to further growth at lower redshifts. While we mention hints favoring one or another of these options, the existing data do not allow us to reach any firm conclusion on this specific issue.

Finally, we point out that while in the local universe most of the most massive galaxies are passively evolving giant ellipticals, the present data, combined with previous evidence in a partly overlapping field (Daddi et al. 2004a, 2004b), indicate that by $z \sim 2$ passively evolving and seemingly vigorous starburst galaxies occur in comparable numbers among most

massive galaxies. This remains a major challenge for the current theoretical simulations of galaxy formation to reproduce.

We thank Swara Ravindranath, Ignacio Trujillo, and Paolo Cassata for providing comments about the morphological analysis, Andrea Comastri for help with Figure 15, and Eros Vanzella for discussions. The anonymous referee is thanked for a careful reading of the manuscript and useful comments. Support for part of this work was provided by NASA through the Spitzer Fellowship Program, under award 1268429. We acknowledge support from the grant GO-09793 from the Space Telescope Science Institute, which is operated by AURA, Inc., under NASA contract NAS5-26555. This project has made use of the aXe extraction software produced by ST-ECF, Garching, Germany.

REFERENCES

Alexander, D. M., et al. 2003, AJ, 126, 539
Avni, Y. 1976, ApJ, 210, 642
Baldry, I. K., Glazebrook, K., Brinkmann, J., Ivezić, Ž., Lupton, R. H., Nichol, R. C., & Szalay, A. S. 2004, ApJ, 600, 681
Bell, E. F., et al. 2004, ApJ, 608, 752
Benítez, N., Broadhurst, T., Bouwens, R., Silk, J., & Rosati, P. 1999, ApJ, 515, L65
Bertin, E., & Arnouts, S. 1996, A&AS, 117, 393
Bolzonella, M., Miralles, J.-M., & Pelló, R. 2000, A&A, 363, 476
Broadhurst, T., & Bouwens, R. J. 2000, ApJ, 530, L53
Brown, M. J. I., Jannuzi, B. T., Dey, A., & Tiede, G. P. 2005, ApJ, 621, 41
Brusa, M., Gilli, R., & Comastri, A. 2005b, ApJ, 621, L5
Brusa, M., et al. 2002, ApJ, 581, L89
———. 2005a, A&A, 432, 69
Bruzual, G., & Charlot, S. 2003, MNRAS, 344, 1000
Calzetti, D., et al. 2000, ApJ, 533, 682
Caputi, K. I., Dunlop, J. S., McLure, R. J., & Roche, N. D. 2004, MNRAS, 353, 30
Cassata, P., et al. 2005, MNRAS, 357, 903
Chen, H.-W., & Marzke, R. O. 2004, ApJ, 615, 603
Cimatti, A., et al. 2002a, A&A, 381, L68
———. 2002b, A&A, 392, 395
———. 2004, Nature, 430, 184
Cole, S., et al. 2001, MNRAS, 326, 255
Conselice, C. J. 2003, ApJS, 147, 1
Daddi, E., Broadhurst, T. J., Zamorani, G., Cimatti, A., Röttgering, H., & Renzini, A. 2001, A&A, 376, 825
Daddi, E., Cimatti, A., Pozzetti, L., Hoekstra, H., Röttgering, H. J. A., Renzini, A., Zamorani, G., & Mannucci, F. 2000a, A&A, 361, 535
Daddi, E., Cimatti, A., & Renzini, A. 2000b, A&A, 362, L45
Daddi, E., Cimatti, A., Renzini, A., Fontana, A., Mignoli, M., Pozzetti, L., Tozzi, P., & Zamorani, G. 2004a, ApJ, 617, 746
Daddi, E., et al. 2003, ApJ, 588, 50
———. 2004b, ApJ, 600, L127
Dressler, A., & Gunn, J. E. 1983, ApJ, 270, 7
Dunlop, J., Peacock, J., Spinrad, H., Dey, A., Jimenez, R., Stern, D., & Windhorst, R. 1996, Nature, 381, 581
Eggen, O. J., Lynden-Bell, D., & Sandage, A. R. 1962, ApJ, 136, 748
Ferguson, H. C., et al. 2004, ApJ, 600, L107
Ferrarese, L., & Merritt, D. 2000, ApJ, 539, L9
Firth, A. E., et al. 2002, MNRAS, 332, 617
Fontana, A., et al. 2004, A&A, 424, 23
Gao, L., Loeb, A., Peebles, P. J. E., White, S. D. M., & Jenkins, A. 2004, ApJ, 614, 17
Gebhardt, K., et al. 2003, ApJ, 597, 239
Georgakakis, A., Afonso, J., Hopkins, A. M., Sullivan, M., Mobasher, B., & Cram, L. E. 2005, ApJ, 620, 584
Giacconi, R., et al. 2002, ApJS, 139, 369
Glazebrook, K., et al. 2004, Nature, 430, 181
Goudfrooij, P., & de Jong, T. 1995, A&A, 298, 784
Granato, G. L., De Zotti, G., Silva, L., Bressan, A., & Danese, L. 2004, ApJ, 600, 580
Granato, G. L., Silva, L., Monaco, P., Panuzzo, P., De Zotti, G., & Danese, L. 2001, MNRAS, 324, 757
Hernandez, X., & Lee, W. H. 2004, MNRAS, 347, 1304
Jorgensen, I., Franx, M., & Kjaergaard, P. 1995, MNRAS, 273, 1097
Kauffmann, G., Colberg, J. M., Diaferio, A., & White, S. D. M. 1999, MNRAS, 307, 529
Kauffmann, G., White, S. D. M., Heckman, T. M., Ménard, B., Brinchmann, J., Charlot, S., Tremonti, C., & Brinkmann, J. 2004, MNRAS, 353, 713
Kong, X., et al. 2005, ApJ, submitted
Kormendy, J. 1977, ApJ, 218, 333
Kurucz, R. L. 1979, ApJS, 40, 1
Loeb, A., & Peebles, P. J. E. 2003, ApJ, 589, 29
Maccacaro, T., Braito, V., Della Ceca, R., Severgnini, P., & Caccianiga, A. 2004, ApJ, 617, L33
Magorrian, J., et al. 1998, AJ, 115, 2285
Maraston, C. 2005, MNRAS, submitted (astro-ph/0410207)
McCarthy, P. J. 2004, ARA&A, 42, 477
McCarthy, P. J., et al. 2001, ApJ, 560, L131
———. 2004, ApJ, 614, L9
Menanteau, F., Abraham, R. G., & Ellis, R. S. 2001, MNRAS, 322, 1
Menanteau, F., et al. 2004, ApJ, 612, 202
Mignoli, M., et al. 2004, A&A, 418, 827
Miyazaki, M., et al. 2003, PASJ, 55, 1079
Moustakas, L. A., & Somerville, R. S. 2002, ApJ, 577, 1
Nagamine, K., Cen, R., Hernquist, L., Ostriker, J. P., & Springel, V. 2005a, ApJ, 618, 23
———. 2005b, ApJ, in press (astro-ph/0502001)
Nolan, L. A., Dunlop, J. S., & Jimenez, R. 2001, MNRAS, 323, 385
Padovani, P., Allen, M. G., Rosati, P., & Walton, N. A. 2004, A&A, 424, 545
Pasquali, A., Pirzkal, N., & Walsh, J. 2003, ST-ECF Instrument Science Report ACS 2003-001, http://www.stecf.org/instruments/acs/ISR/isr0301.pdf
Peng, C. Y., Ho, L. C., Impey, C. D., Rix, H.-W. 2002, AJ, 124, 266
Pirzkal, N., et al. 2004, ApJS, 154, 501
———. 2005, ApJ, 622, 319
Pozzetti, L., & Mannucci, F. 2000, MNRAS, 317, L17
Pozzetti, L., et al. 2003, A&A, 402, 837
Quintero, A. D., et al. 2004, ApJ, 602, 190
Ravindranath, S., Ho, L. C., Peng, C. Y., Filippenko, A. V., & Sargent, W. L. W. 2001, AJ, 122, 653
Renzini, A. 2005, in IMF at 50, ed. E. Corbelli, F. Palla, & H. Zinnecker (Dordrecht: Kluwer), in press (astro-ph/0410295)
Roche, N. D., Almaini, O., Dunlop, J., Ivison, R. J., & Willott, C. J. 2002, MNRAS, 337, 1282
Saracco, P., et al. 2005, MNRAS, 357, L40
Sérsic, J. L. 1968, Atlas de Galaxias Australes (Córdoba: Observatorio Astronomico, Univ. Nacional de Córdoba)
Smith, G. P., Treu, T., Ellis, R., Smail, I., Kneib, J.-P., & Frye, B. L. 2001, ApJ, 562, 635
Somerville, R. S., Primack, J. R., & Faber, S. M. 2001, MNRAS, 320, 504
Somerville, R. S., et al. 2004, ApJ, 600, L135
Spergel, D. N., et al. 2003, ApJS, 148, 175
Spinrad, H., Dey, A., Stern, D., Dunlop, J., Peacock, J., Jimenez, R., & Windhorst, R. 1997, ApJ, 484, 581
Springel, V., Di Matteo T., & Hernquist, L. 2005, ApJ, 620, L79
Stanford, S. A., Dickinson, M., Postman, M., Ferguson, H. C., Lucas, R. A., Conselice, C. J., Budavári T., & Somerville, R. 2004, AJ, 127, 131
Stiavelli, M., et al. 1999, A&A, 343, L25
Stockton, A., Canalizo, G., & Maihara, T. 2004, ApJ, 605, 37
Strateva, I., et al. 2001, AJ, 122, 1861
Szokoly, G. P., et al. 2004, ApJS, 155, 271
Thomas, D., Maraston, C., & Bender, R. 2002, Rev. Mod. Astron., 15, 219
Thomas, D., Maraston, C., Bender, R., & Mendes de Oliveira, C. 2005, ApJ, 621, 673
Toomre, A. 1977, in Evolution of Galaxies and Stellar Populations, ed. B. M. Tinsley & R. B. Larson (New Haven: Yale Univ. Observatory), 401
Treu, T., Ellis, R. S., Liao, T. X., & van Dokkum, P. G. 2005, ApJ, 622, L5
Treu, T., Stiavelli, M., Casertano, S., Møller, P., & Bertin, G. 1999, MNRAS, 308, 1037
van der Marel, R. P. 1991, MNRAS, 253, 710
van Dokkum, P. G., et al. 2004, ApJ, 611, 703
Waddington, I., et al. 2002, MNRAS, 336, 1342
Xu, C., et al. 2005, ApJ, submitted
Yan, H., et al. 2004a, ApJ, 616, 63
Yan, L., Thompson, D., & Soifer, B. T. 2004b, AJ, 127, 1274
Zheng, W., et al. 2004, ApJS, 155, 73
Ziegler, B. L., Saglia, R. P., Bender, R., Belloni, P., Greggio, L., & Seitz, S. 1999, A&A, 346, 13